

Theoretical aspects of highly correlated fullerides: metal-insulator transition

Nicola Manini^{1,2} and Erio Tosatti^{2,3,4}

¹ Dipartimento di Fisica, Università di Milano,
Via Celoria 16, 20133 Milano, Italy

² International School for Advanced Studies (SISSA),
Via Beirut 4, 34014 Trieste, Italy

³ INFN Democritos National Simulation Center,
Via Beirut 4, 34014 Trieste, Italy

⁴ International Centre for Theoretical Physics (ICTP),
P.O. Box 586, I-34014 Trieste, Italy

Summary. We review some theoretical aspects connected with the interplay of strong electron correlations and vibron phenomena in negative fullerene ions and in solid fulleride conductors, superconductors and insulators. The first part covers molecular ions, their intra-molecular Jahn-Teller effect, Coulomb (Hund's rule) exchange interactions, molecular vibrons and multiplet splittings. The second part addresses electron propagation in molecular fullerides, with special emphasis given to trivalent cases such as K_3C_{60} and $NH_3 K_3C_{60}$, where metallic, superconducting and Mott insulating phases are at play. Dynamical mean field theory approaches to a simplified Hamiltonian for this system are discussed in the light of some of the observed phenomenology. It is argued in particular that $NH_3 K_3C_{60}$ is a Mott-Jahn-Teller insulator, which under pressure turns into a strongly correlated superconductor, thus sharing some important elements with the high- T_c cuprates.

6.1 Introduction

The wealth of experimental data on the alkali fullerides collected through the 1990s and early 2000s has raised several exciting theoretical issues which, in turn, have attracted a large research effort. Different phases are realized when temperature, alkali concentration, lattice parameter and lattice structure are varied. Metallic, insulating, and superconducting phases are obtained in solid compounds characterized by the partial occupancy – by an average n electrons per C_{60} with n ranging between 0 and 6 – of the narrow electronic band originating from the t_{1u} LUMO molecular orbital. When this band is completely empty (pure C_{60}) or completely filled (K_6C_{60}) the solid is a band insulator (although the lattice structure in the two solids are different). Band-structure calculations of compounds characterized by an incomplete filling of this band consistently predict metallicity [1, 2, 3]. However, experimentally some of these compounds (e.g. K_4C_{60} , Rb_4C_{60} , $NH_3 K_3C_{60}$) are found to be

insulators [4, 5, 6, 7, 8, 9, 10]. Among the metallic compounds, many with $n = 3$ turn superconducting at low temperature, with transition temperatures as high as 30 – 40 K, while several others remain metallic at all experimentally investigated temperatures.

For even n , as in K_4C_{60} , electron-electron correlations and the JT coupling stabilize a *correlated insulating state* of a lattice of evenly-charged C_{60} molecules. In this type of insulator, fluctuations about $\langle n_i \rangle = n$ are suppressed, and a gap opens in the electronic spectrum. This state is non-magnetic, very much like a regular band insulator. However, the mostly intra-molecular electron correlations responsible for band narrowing and gap opening are largely *coulombic* and *vibronic* in origin. We have suggested that the (body-centered tetragonal [11]) structure of K_4C_{60} and Rb_4C_{60} may be a realization of this state where electronic and vibronic interactions play an important role. Similarly, the insulating state observed in strongly correlated $NH_3 K_3C_{60}$ (and $(NH_3)_6 Li_3C_{60}$ [12]) as well as the insulator-superconductor transition obtained under pressure are likely to have the same origin.

A satisfactory understanding of how similar physical parameters lead to very different ground states (insulator/metal/superconductor) has long eluded the research community. A novel picture relating the transitions between metallic, insulating, and superconducting phases to the interplay of strong electron-electron correlation with electron-phonon coupling in the LUMO band has emerged in recent years. The scenario is now in our view better understood, even though many quantitative details still escape the full grasp of theory. The present Chapter reviews and illustrates this picture.

6.2 C_{60} molecules and molecular ions

We review for a start some basic aspects of the physics of C_{60} , concerning electron-electron correlation and electron-vibration coupling in C_{60} molecular ions and ionic fullerenes. For more complete reviews we suggest consulting Refs. [13, 14, 15, 16].

In C_{60} all the 60 carbon atoms of fullerene are arranged as a regular, icosahedral, roughly spherical cage, of ~ 0.7 nm in diameter [17]. This cluster may be thought as a piece of graphene sheet, wrapped up to a spherical shape. The regular hexagonal structure of graphite is distorted, with 12 five-membered rings intercalating 20 six-membered ones, thus introducing the Eulerian 4π solid angle necessary to yield a closed surface. The order is such that all carbon atoms remain equivalent, each sitting at the corner of one 5-member ring and two 6-member ones. 30 chemical bonds, the so-called double bonds, are shared by two hexagonal rings only; the remaining 60 bonds, shared by pentagonal and hexagonal rings, are about 5% longer [18]. The σ -bonding sp^2 graphite orbitals constitute the backbone of the molecule. Spherical curvature alters their character to an average "sp^{2.28}" [19]. In energy, the σ -bonding orbitals range from several eV to a few tens of eV below the vacuum, the antibonding states lying +10 eV and higher above vacuum zero [20]. The chemically active electronic states are those derived from the "p_z" carbon orbitals (actually of hybrid "s^{0.09}p" nature [19]) that are directed radially, supporting a half filled π -electron system.

Although theoretically metastable compared to graphite and diamond, C_{60} is nevertheless an empirically very stable and long lived allotropic form of carbon both as an isolated molecule and as an fcc, or Pa3, solid. The reason for stability is

the substantial amount of electronic energy gained in the delocalized MO's, making in some sense C_{60} the spherical counterpart of the aromatic benzene ring. The molecular orbitals at the origin of the conduction bands of solid fullerenes are all of π -bonding/antibonding nature.

The overall molecular symmetry group is the icosahedral group I_h , the largest point group in 3D (except for axial groups). Symmetry implies a large degeneracy of the group's irreducible representations [21]: $A_{g/u}$ (1-dimensional), $T_{1g/u}$, $T_{2g/u}$ (3-dimensional), $G_{g/u}$ (4-dimensional), and $H_{g/u}$ (5-dimensional). Large degeneracies are accordingly very common to all electronic, vibrational, vibronic molecular states. This makes C_{60} a rich playground of novel vibronic structures, where Berry phases and entanglement plays a fascinating role [22, 23, 24, 25, 26, 27, 28, 29, 30, 31, 32].

Icosahedral symmetry is of course restricted to the ideal situation of a molecule or molecular ion in vacuum. In compounds and/or in the solid state it will be affected by crystal fields of lower symmetry. Even in vacuum, isotope substitution of one carbon atom is enough to reduce I_h to simple bilateral reflection C_v . Due to 1.10% isotope abundance of ^{13}C in natural carbon, only about 50% of C_{60} is pure $^{12}\text{C}_{60}$. However, isotope substitution induces only small splittings (about 1%) of the vibron frequencies, and can be safely neglected for many purposes. For a discussion of the intricacies of isotope shifts in solid-state properties of the fullerenes, see Ref. [16].

As mentioned, immersion of the icosahedral molecule in a solid-state environment reduces its symmetry to that of the local crystal field. For example, solid C_{60} has electronic bands and optical phonons compatible with the local cubic field induced by the fcc lattice. In most (but not all) solid state compounds, intermolecular interactions are relatively loose, each molecule retaining its close structure. Accordingly, splittings of the molecular vibrations (now optical phonons in the solid) due to reduced symmetry are small and hardly observed at all [33].

6.2.1 Molecular electronic states

Electrons in the π orbitals of C_{60} represent the chemically relevant region of the spectrum. These orbitals provide the basic one-electron picture, neglecting first e-e correlation effects, which we shall address in Sec. 6.2.4.

Many approaches have been taken to the electronic structure of C_{60} , from simple Huckel tight-binding with one orbital per atom (already yielding the correct order of molecular energies and gaps) [20, 34, 19], to more extended bases [20, 35] to microscopic DFT-LDA (density functional theory in the local density approximation) calculations on localized [20, 36] and extended bases [1, 37].

These approaches provide an increasing degree of quantitative accuracy in the description of the electronic spectrum. Simple intuitive models, such as the particle-on-a-sphere model [38], are often sufficient for a qualitative and synthetic understanding of the electronic structure. In this approximation the idea is treating the π electrons as though moving on a spherical shell of radius R , mimicking the attractive potential generated by the carbon ions. The precise localization of these ions produces then a weak icosahedral perturbation. As long as this icosahedral perturbation can be neglected, the single-electron angular wavefunctions are atomic-like spherical harmonics Y_{LM} , with energy

$$E(L) = \frac{L(L+1)\hbar^2}{2m_e R^2}, \quad (6.1)$$

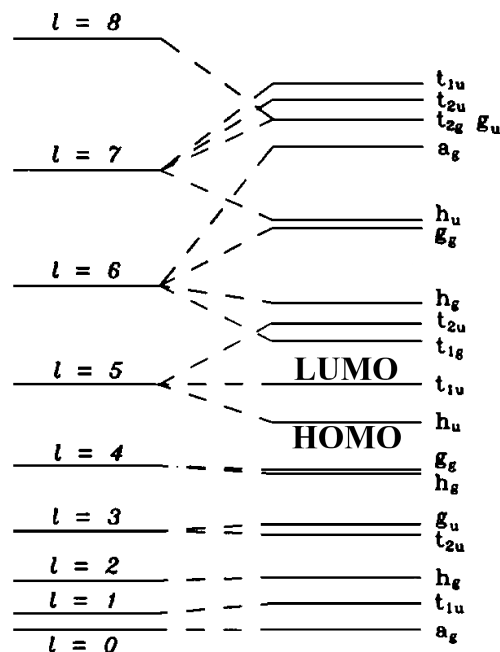


Fig. 6.1. A particle-on-a-sphere schematic representation of the electronic levels of C_{60} . The HOMO and LUMO levels, originating from the $L = 5$ orbital, are indicated. (Adapted from Ref. [38].)

where m_e is the electron mass. 50 out of 60 p_z electrons of the neutral molecule fill completely the MO up to $L = 4$. The lowest $L = 0, 1, 2$ orbitals coincide with icosahedral states labelled a_g, t_{1u}, h_g respectively. All higher L values are split into icosahedral representations by the icosahedral field generated by the cage. After filling all states including $L = 4$, 10 electrons are left in the $L = 5$ shell, which is therefore only partly filled. As it happens, the icosahedral splitting ($L = 5 \rightarrow h_u + t_{1u} + t_{2u}$) of this 11-fold degenerate orbital generates a closed-shell configuration, as shown in Fig. 6.1. In accord with microscopic calculations and with experiment, the completely-filled HOMO has h_u symmetry, and the LUMO is t_{1u} . The HOMO-LUMO gap is therefore caused by the icosahedral perturbation in the $L = 5$ shell, and is experimentally ~ 1 eV for molecules in vacuum [39]. A t_{2g} LUMO+1 state, originated from the $L = 6$ shell, is found approximately 1 eV above the t_{1u} LUMO.

The electron affinity of C_{60} is large (2.69 eV) [40, 41] and experimental evidence has been found that C_{60}^- [42] and even C_{60}^{2-} [43] are stable ions in vacuum. In solution, a wider spectrum of ionization states has been demonstrated electrochemically, up to C_{60}^{6-} [44, 45, 46, 47]. As an adsorbate on a metal surface, the electronegative C_{60} molecule naturally picks up electrons [1, 48], and evidence has been provided of charge transfer as large as $n=6$ [49]. In the solid state, compounds have been synthesized, covering a wide range of charge transfers, from $n=1$, as in TDAE- C_{60} [50, 51] or Rb_1C_{60} [4], $n=3$, as in K_3C_{60} or Rb_3C_{60} [52], $n=4$ as in K_4C_{60} [53], $n=6$ as in Rb_6C_{60} [54], or even higher as in $Li_{12}C_{60}$ [55, 56]. More recently, also

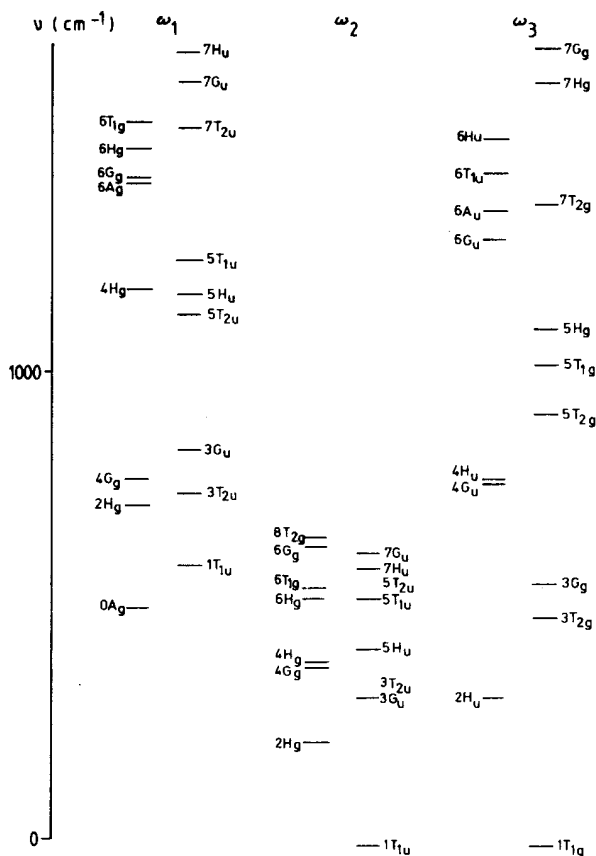


Fig. 6.2. Spherical resolution of the vibrational spectrum of C_{60} . The modes are organized according to the three series, indicated with $\omega_{1/2/3}$. The spherical parent L is indicated before the icosahedral label. (From Ref. [65]).

positive C_{60} ions were produced in gas phase [57], in liquid solution [58, 59], in Ar matrix [60], and in the solid state [61, 62, 63, 64]. Since the LUMO can hold up to 6 electrons, the negatively charged ions C_{60}^{n-} with $1 \leq n \leq 5$ are open shells. Likewise, the cations C_{60}^{n+} with $1 \leq n \leq 9$ are also open shells due to the fivefold degeneracy of the HOMO orbital.

6.2.2 Molecular vibrations

C_{60} has 174 vibrational degrees of freedom, but thanks to symmetry-induced degeneracy and selection rules, the vibrational spectra show relatively few peaks, with clear identification. In particular, only the 4 T_{1u} dipolar modes are infrared active, and only the 2 A_g and 8 H_g modes are Raman active. Neutron experiments [66] are sensitive to all modes, including the silent ones, but with low resolution. Cal-

culations are therefore crucial, in order to get a global picture of the vibrational spectrum [65].

Like for the electronic states, many routes to the calculation of vibrational eigenfrequencies and normal modes have been pursued, both based on force field fits to the experimentally accessible data [66, 67, 68], or based on *ab initio* calculations of the molecular structure [35, 37, 69, 70]. The agreement among different calculations is somewhat worse than for the electronic levels: typical discrepancies on the order of several meV are well above nowadays' experimental resolution.

A qualitative understanding of the vibrational structure of C_{60} is provided by the analogy of the C_{60} cage with a hollow elastic sphere proposed in Ref. [65] and illustrated in Fig. 6.2. The eigenmodes of a homogeneous spherical membrane with a stretching and a bending rigidity are collected in three classes: mainly radial, mainly tangential and purely tangential. The first class contains levels of parity $(-1)^L$, with $L = 0, 1, 2, 3, \dots$; the levels in the second class have the same parity, but start off at $L = 1$; in the third series the parity is reversed $(-1)^{L+1}$, and they start at $L = 1$. The modes of rigid translation and rotation of the sphere are identified in the $L = 1$ states at zero frequency in series 2 and 3. Of course, when the homogeneous sphere is replaced by the discrete 60-atoms molecule, the infinite set of spherically symmetric eigenmodes goes into a finite number of modes, now labeled by \mathcal{I}_h representations. $L = 0, 1, 2$ states have icosahedral counterparts in $A_{g/u}$, $T_{1u/g}$, $H_{g/u}$ respectively: the first *gerade/ungerade* label corresponds to series 1 and 2, the second labels the third series, which has inverted parity. States with $L > 2$ are split, according to the rules given in Table III of Ref. [65]; for example a $L = 3$ vibration becomes $T_{2u} \oplus G_u$, if its parity is odd. The explicit eigenmodes, computed for example by force-field methods, can be easily analyzed in terms of the spherical basis, to obtain their parentage in terms of hollow sphere modes [65]: the three series are readily identified in Fig. 6.2. Inter-mode mixing is present, but most vibrations hold a well-defined spherical parentage, so that the spherical picture remains generally valid and useful.

6.2.3 Jahn-Teller coupling between electrons and vibrations: molecular vibronic states and energetics

The electronic state of most $C_{60}^{n\pm}$ ions is orbitally degenerate. According to the Jahn-Teller (JT) theorem, the highly symmetric \mathcal{I}_h geometry is unstable toward symmetry reducing molecular distortions. Theoretically, such distortion can be evaluated by direct calculation of the relaxed geometry of the molecular ions, and are very well defined. However, direct experimental evidence of the JT distortions is rather poor, and limited to few compounds, mainly "discrete" salts, as discussed in detail in Ref. [15]. The reason for this is twofold: (i) the atomic displacements from the \mathcal{I}_h positions of neutral C_{60} are very small – of the order of few pm, and (ii) quantum tunneling and/or thermal hopping of the molecule between equivalent JT distortions generally restores, on average, the original \mathcal{I}_h symmetry.

Despite the small absolute atomic displacements, the JT physics involves serious energetics, since the phonon frequencies are high (owing to the large stiffness of the fullerene cage and the light carbon mass) and the JT couplings are large. At zero temperature, a significant fraction of the JT energy is associated to nonadiabatic effects related to the quantum motion of carbon nuclei, and cannot be obtained by

standard adiabatic calculations based on *classical* atomic positions. However, quantitative insight in the coupled electron-phonon dynamics is obtained by means of the study of formally simple models. To the extent that these distortions are not too large, the distortion mechanism is well described within a model where the distortion is expanded on the basis of the normal modes of vibration: these are treated as harmonic oscillators, and the coupling between the degenerate electron level and the JT-active distortions can be assumed to be linear in the phonon coordinate. These simplifying approximations remain valid only as long as the distortions are relatively small, as in C_{60} ions, and could not be applied to ionic states of e.g. SiH_4 , whose molecular shape is radically modified upon charging [71].

The basic model Hamiltonian for the JT dynamics of an icosahedral molecule has the following standard structure [72]:

$$\hat{H} = \hat{H}_0 + \hat{H}_{e-v}, \quad (6.2)$$

where \hat{H}_0 describes the free (uncoupled) electrons and vibrations and \hat{H}_{e-v} the linear JT interaction. To begin with, consider a single vibrational mode of energy $\hbar\omega$ and symmetry label Λ : the Hamiltonian are written

$$\hat{H}_0 = \hbar\omega \sum_{\mu \in \Lambda} \left(\hat{b}_\mu^\dagger \hat{b}_\mu + \frac{1}{2} \right) + (\epsilon - \mu) \sum_{m \in \lambda} \sum_{\sigma = \uparrow, \downarrow} \hat{c}_{m, \sigma}^\dagger \hat{c}_{m, \sigma}, \quad (6.3)$$

$$\hat{H}_{e-v} = g\hbar\omega \frac{\sqrt{3}}{2} \sum_{m_1, m_2 \in \lambda} \sum_{\mu \in \Lambda} C_{\lambda m_1 \lambda m_2}^{\Lambda, \mu} \left(\hat{b}_\mu^\dagger + \hat{b}_\mu \right) \hat{c}_{m_1 \sigma}^\dagger \hat{c}_{-m_2 \sigma}. \quad (6.4)$$

Here, the harmonic oscillator is represented by the boson operators b_μ^\dagger : the indexes μ span the degenerate representation Λ . The distortion coordinate appears in the coupling term (6.4) as $\hat{Q}_\mu = 2^{-1/2} (\hat{b}_\mu^\dagger + \hat{b}_\mu)$. $\lambda = t_{1u}$ is the symmetry label of the LUMO electronic state, span by indexes m_i and generated by the fermion operators $\hat{c}_{m \sigma}^\dagger$. g is the dimensionless parameter measuring the electron-vibration coupling strength. $C_{\lambda m_1 \lambda m_2}^{\Lambda, \mu}$ is a Clebsch-Gordan coefficient for the icosahedral-group [73], which recouples the fermion tensors of λ symmetry with the boson tensor to an icosahedral scalar. In practice, this recoupling is possible only for modes of symmetry $\Lambda = A_g, H_g$. All other Λ 's yield vanishing Clebsch-Gordan coefficients, which means that all modes of non- A_g/H_g symmetry are not linearly coupled to the t_{1u} LUMO.

It is interesting to note that the \mathcal{I}_h Clebsch-Gordan coefficients for the coupling of two t_{1u} representations to $\Lambda = A_g/H_g$ happen to coincide numerically with the corresponding $C_{l m_1 l m_2}^{L, \mu}$ Clebsch-Gordan coefficients for the full rotations group $SO(3)$. The t_{1u} label maps to angular momentum $l = 1$, while A_g maps to $L = 0$, and H_g maps to $L = 2$, in accord with the spherical picture of Figs. 6.1 and 6.2. This means physically that linear JT coupling of the t_{1u} orbital does not distinguish between a soccer-ball molecule and a perfectly spherically shaped one: the t_{1u} level behaves as an atomic-like p state perturbed by A_g/H_g distortions of monopolar and quadrupolar nature [72, 74, 75]. The implications of this extra symmetry are striking: Hamiltonian (6.2) is actually a scalar with respect to the full rotation group $SO(3)$, its eigenstates being representations of this larger group. $SO(3)$ states are to be expected in the outgoing spectrum, which means that vibronic states belonging to different \mathcal{I}_h representations collapse to degenerate $SO(3)$ multiplets (labeled by some angular momentum L , rather than by \mathcal{I}_h labels), as on the left side of Fig. 6.1. In actual C_{60} , the linear electron-vibration coupling term is just the leading term in

an infinite expansion, where only higher-order terms introduce the actual icosahedral symmetry, thus splitting the highly degenerate spherical vibronic states not unlike Fig. 6.1. Eventually, the effect of these higher-order terms is small, yielding very small splittings of the vibronic states: neglect of all these higher-order effects is a good approximation for C_{60}^{n-} .

Electron coupling to the $A = A_g$ mode represents a trivial shifted oscillator, since the nondegenerate mode does not split the electronic degeneracy, and the distortion is purely proportional to the total charge in the coupled level. Henceforth we shall mostly concentrate on coupling to degenerate $A = H_g$ modes.

There is no loss of generality in choosing the energy reference so that $\epsilon = \mu$ in Eq. (6.3). We are then left with a two-parameters Hamiltonian operator. The value $\hbar\omega$ of the frequency of the harmonic oscillator sets the energy scale. \hat{H}_0 and \hat{H}_{e-v} are written with a common factor $\hbar\omega$, which sets the energy scale of the model. The dimensionless parameter g tunes the intensity of the JT coupling, thus of the tendency of the system to distort. This is seen as follows: express each pair of vibrational operators ($\hat{b}_\mu^\dagger, \hat{b}_\mu$) as a dimensionless coordinate \hat{Q}_μ and conjugate momentum \hat{P}_μ . In this notation, the adiabatic potential is obtained by ignoring the $\frac{1}{2} \sum \hat{P}_\mu^2$ phonon kinetic term in \hat{H}_0 and treating the \hat{Q}_μ operators as classical variables Q_μ [76]: one readily finds that $Q_0 = g$ (all other $Q_\mu = 0$) is a minimum of the sum of the competing Q_μ -linear term (\hat{H}_{e-v}) and Q_μ -quadratic term in \hat{H}_0 . We see here that g measures the amount of distortion (in dimensionless oscillator coordinates) along the normal mode. For small $g \ll 1$ (weak-coupling regime) distortions are small. In this regime quantum fluctuations dominate: the correlated vibrational and electronic dynamics involves all electronic states in the multiplet at the same time, in a profoundly nonadiabatic fashion. Despite this intricacy, as a small parameter can be identified, the JT problem can be dealt with by treating \hat{H}_{e-v} by perturbation theory. For intermediate $g \simeq 1$, the distortion is sizeable, but quantum kinetic energy has a relevant role in promoting tunneling among equivalent minima. The vibronic spectrum in this region shows nontrivial structures. Eventually, when the coupling becomes very large ($g \gg 1$), the JT distortion is so large that individual JT minima remain well separate so that tunneling is efficiently suppressed: the system freezes in one of the equivalent local minima.

Here we should note a peculiarity of the so-called linear $t \otimes H$ JT problem Eq. (6.3)-(6.4) at hand, and precisely that the minimization of the lowest adiabatic potential sheet leads to a continuous manifold of equivalent minima (a *trough*) rather than isolated minima [22, 23, 72]. This is a consequence of the extra spherical symmetry of this special icosahedral linear JT system. However, at strong coupling higher-than-linear terms, neglected in Eq. (6.4) become relevant. They produce a warping of the JT trough, leading to isolated minima. The molecule distorts to a minimum in a set of static JT reduced-symmetry configurations separated by saddle points of the adiabatic potential surface. For the intermediate coupling case of C_{60}^- , detailed Hartree-Fock calculations have shown, for example, that the total energy lowering in going from the \mathcal{I}_h -symmetric molecular configuration to static JT distortions of D_{5d} , D_{3d} , D_{2h} symmetries, are in fact identical to within 1% [77]. Therefore, the linear JT coupling approximation Eq. (6.4) is very well justified for C_{60} ions.

Analytical expression for the $t \otimes H$ JT energies can be obtained in the simple weak-coupling limit, by means of perturbation theory [23]. The main outcome of the weak-coupling regime is that the ground-state energy gain E^{e-v} in this JT system

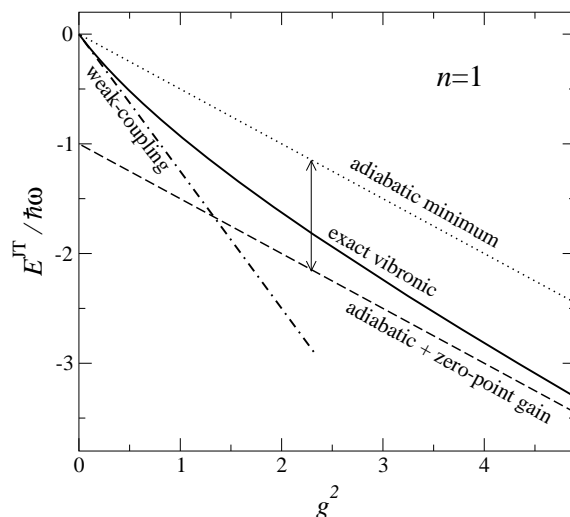


Fig. 6.3. Ground-state energy lowering for a t_{1u} electron coupled to an H_g mode as a function of coupling. At weak coupling (dot-dashed), the ground-state energy (solid) drops 2.5 times more rapidly than the adiabatic minimum lowering (dotted) in order to reach the correct strong-coupling semiclassical limit (dashed), which takes into account the softening of two (for $n = 1$) harmonic modes for a total zero-point gain $\hbar\omega$ (indicated by a vertical arrow). (Adapted from Ref. [78].)

is 5/2 times larger in perturbation theory than the simple adiabatic lowering [79]. This point is illustrated in Fig. 6.3 for $n = 1$. For a simple nondegenerate non-JT coupling, such as that to the A_g mode, the two quantities would instead coincide. The physical origin of this enhancement is a substantial reduction in zero-point energy. The ground-state energy drops faster at small g because the system transforms rapidly from 5 harmonic oscillators (zero-point energy = $\frac{5}{2}\hbar\omega$) at $g = 0$ to a Mexican-hat potential well, which is more “square-well”-like than the original harmonic potential, and, in particular, carries several soft (“pseudorotational”) modes along the trough. Perturbative expressions for the ground-state energy lowering at weak coupling for $t_{1u}^n \otimes H$ in all possible spin states are collected in Table 6.1. The perturbative expressions are essentially exact for $g \leq 0.3$. For larger (intermediate) coupling, the actual JT energy lowering is located between the perturbative “antiadiabatic” estimate (which systematically overestimates the JT energy lowering) and the adiabatic energy lowering (which consistently underestimates the energy lowering).

In the strong-coupling limit, E_n^{e-v} coincides with the classical adiabatic energy lowering (proportional to $g^2\hbar\omega$), with the addition of a negative zero-point softening contribution (of order $\hbar\omega$). As was the case at weak coupling, in multi-electron contexts, JT distortions leads to a larger energy gain when charge concentrates in as few orbital as possible, thus favoring larger distortions. Due to this, low-spin configurations end generally lower in energy than high spin ones, giving rise to a kind of reversed (first) Hund’s rule exchange behavior (here we ignore the actual Hund rule, which is however important, and will be introduced in Sec. 6.2.4). To describe

Table 6.1. Perturbative (weak coupling, to order g^2 [23]) and semiclassical (strong coupling, to order g^{-2} [72]) ground-state energies for an H_g mode coupled to n electrons in a t_{1u} orbital, for the allowed values of the total spin S . Here, only electron-phonon coupling is considered, while electron-electron repulsion is neglected.

C_{60}^{n-}	spin	$E_n^{e-v}/(\hbar\omega)$ [for $g \rightarrow 0$]	$E_n^{e-v}/(\hbar\omega)$ [for $g \rightarrow \infty$]	Berry phase γ	ground-state symmetry
0	0	0	0	0	A_g
1	$\frac{1}{2}$	$-\frac{5}{4}g^2$	$-\frac{1}{2}g^2 - 1 + \frac{1}{3}g^{-2}$	π	T_{1u}
2	0	$-5g^2$	$-2g^2 - 1 + \frac{1}{12}g^{-2}$	0	A_g
2	1	$-\frac{5}{4}g^2$	$-\frac{1}{2}g^2 - 1 + \frac{1}{3}g^{-2}$	π	T_{1g}
3	$\frac{1}{2}$	$-\frac{15}{4}g^2$	$-\frac{3}{2}g^2 - \frac{3}{2} + \frac{3}{8}g^{-2}$	π	T_{1u}
3	$\frac{3}{2}$	0	0	0	A_u

correctly the quantum dynamics in the JT trough, a detailed analysis of the coupled electron-phonon system is needed. A crucial ingredient in this problem is the value 0 or π of an electronic Berry phase [22, 24, 80, 81, 82] γ in the semiclassical motion: it imposes the boundary condition on the soft-mode pseudorotational dynamics in the trough, thus selecting vibronic states of a given parity $\exp(i\gamma)$ [22, 75], not unlike similar vibronic contexts [83, 84, 85, 86]. This boundary condition determines the leading corrections to the adiabatic energetics, of order $\hbar\omega/g^2$, reported in Table 6.1 [72].

The model Hamiltonian (6.2) is readily extended to include all vibrational modes of real C_{60} . Each mode adds one harmonic term of the type (6.3) and a coupling term of the type (6.4), characterized by an individual coupling amplitude g_k and frequency ω_k . In the evaluation of the total electron-phonon coupling, one should also include two A_g vibrons which also couple linearly to the LUMO electrons, even though they do not split its degeneracy. This is a simple polaron problem, which is exactly solvable [87] and independent from the $t_{1u} \otimes 8H_g$ problem. The amount of A_g -related electron-phonon energy is simply $-n^2 g^2 \hbar\omega/2$, independent of the total spin S .

Coming to the eight H_g modes, generally speaking, even within the harmonic-phonon linear-coupling approximation, a realistic description of the dynamical JT state of a C_{60}^{n-} ion is a significantly more complicated affair than the single-mode problem. Linear superposition of in the coupling of individual H_g modes to a *same* t_{1u} orbital is valid only in the antiadiabatic perturbative regime, but does not seriously apply to the coupling range generally accepted for C_{60} : for a general coupling strength, there is in fact no linear superposition. The JT splitting of the LUMO increases with the cooperative action of the single modes, so that even moderate coupling of many individual modes builds up a rather strong total coupling.

For the detailed values of the electron-phonon couplings, several estimates are available in the literature [33, 35, 36, 70, 88, 89, 90, 91, 92, 93], some of which are reported in Table 6.2. The main observation here is that individual mode couplings are indeed intermediate to weak. However, a significant spread in the values of different estimates is due to the large sensitivity of the coupling to the individual phonon eigenvector, which differ largely in different approximations. Moreover, the total coupling of all calculations is significantly weaker than all experimental

Table 6.2. Dimensionless couplings g_k for the eight H_g modes to the LUMO of C_{60} , according to several theoretical and experimental determinations. In the literature, the electron-phonon coupling are often gauged in terms of the weak-coupling superconductivity parameter λ : the relation with the Hamiltonian coupling strengths g_k is [88]: $g_k^2 = \frac{6}{5}\lambda_k/N(\epsilon_F)/\hbar\omega_k$ for the H_g modes (where $N(\epsilon_F)$ is the density of states per C_{60} at the Fermi energy ϵ_F ; one would get $g_k^2 = 3\lambda_k/N(\epsilon_F)/\hbar\omega_k$ for the A_g modes). $g_{\text{eff}}^2 = \sum_k g_k^2$ measures the total interaction strength, and $w_{\text{eff}} = \sum_k g_k^2 w_k / g_{\text{eff}}^2$ provides and average phonon frequency to estimate zero-pint effects. The last line reports the total $\lambda/N(\epsilon_F)$ from H_g modes, according to the different estimates.

H_g mode	$\hbar\omega_k$ [33]	Varma [89]	Schlüter [88]	Antropov [90]	Faulhaber [91]	Manini [70]	Raman [92]	PES [93]
k	[meV]	g_k		–	dimensionless			
1	34	0.326	0.533	0.326	0.188	0.421	1.300	0.821
2	54	0.149	0.394	0.365	0.471	0.494	0.666	0.941
3	88	0.117	0.234	0.202	0.117	0.350	0.202	0.421
4	96	0	0.296	0.194	0.354	0.224	0.194	0.474
5	136	0.230	0.094	0.163	0.133	0.188	0.094	0.325
6	155	0	0.152	0.249	0.124	0.152	0.088	0.197
7	177	0.480	0.297	0.368	0.319	0.319	0.165	0.339
8	195	0.260	0.235	0.368	0.235	0.293	0.136	0.376
tot H_g :								
g_{eff}^2	$\sum_k g_k^2$	0.493	0.756	0.677	0.586	0.840	2.285	2.363
$\hbar w_{\text{eff}}$	[meV]	136	83	121	102	93	44	75
$\lambda/N(\epsilon_F)$	[meV]	56	52	68	49	65	83	147

estimates, such as those obtained by fitting the vibronic features of the photoemission spectrum of C_{60}^- [93]. This is rather surprising in view of the fact that a recent parameter-free calculation [94, 95, 96] found instead good accord with observed vibronic structures in photoemission data of neutral C_{60} [97, 98], based on HOMO couplings computed [70] with the same *ab-initio* techniques as those for the LUMO reported in Table 6.2. Even though some ideas are being pursued to understand the theory-experiment discrepancy for the LUMO couplings [99], this is still an unresolved issue.

As pointed out by Bergomi and Jolicoeur [100], experiments on anions in matrix may yield relevant information to the vibronic effects. Near-infrared and optical spectra of C_{60}^{n-} ions in solution and frozen Ar are available [45, 101]. A major $t_{1u} \rightarrow t_{1g}$ optical transition near 1 eV is present for all values of n . It is accompanied by additional vibronic shake-up structures, typically near 350, 750, 1400 and 1600 cm^{-1} , which involve the vibronic couplings of both the t_{1u} LUMO and t_{1g} LUMO+1. Also, a satisfactory vibronic assignment of a recently observed gas-phase spectrum [39] is not yet available. The experimental information seems insufficient as yet for any relevant comparison with our calculations. Well-defined vibrational spectra are instead available for chemisorbed C_{60}^{n-} [49] and for $A_n C_{60}$ alkali fullerenes [54]. In this case, however, interaction of the electronic t_{1u} level with surface states or with other t_{1u} states of neighboring balls turns the level into a broad band, and our treatment as it stands is invalid. Rapid electron hopping from a molecule to another interferes substantially with the dynamical JT process, in a way which is not known

in detail [76, 102, 103]. The spectra of negatively charged C_{60} adsorbates and solids, in any case, do not present any clear evidence of vibronic splittings, but rather of the gradual continuous shift most likely due to a gradual overall change of geometry, also suggested by DFT-LDA calculations [37].

The full quantum-mechanical problem of a threefold degenerate electronic state linearly coupled to eight fivefold degenerate harmonic oscillators is conceptually simple but in practice, for arbitrary couplings, rather hard to solve exactly. On one side, it is straightforward to compute the Hamiltonian matrix elements on a truncated oscillator basis. Also, this matrix is sparse, involving nonzero terms only between states whose numbers of vibrons differ by exactly one. Moreover, the inclusion of states with up to N vibrons, because of linear e-v coupling, implies decay as $\exp(-N)$ of components with N -vibron states, for large enough N . For this reason, a truncated basis set including all states up to N^{\max} vibrons gives a variational estimate of the lowest eigenvalues, with good convergence with increasing N^{\max} [22, 25, 95]. The structure of the problem makes it especially suitable for a Lanczos algorithm. By this numerical technique, not only the ground-state energy but also several low-lying excitations can be computed [104].

To get an estimate of the accuracy of the adiabatic and antiadiabatic approximations applied to C_{60}^- , the couplings of Ref. [70] (see Table 6.2) can be plugged in the strong and weak-coupling formulas of Table 6.1 and obtain the following estimates for the ground-state energy: $E_{\text{ad } 1}^{\text{e-v}} = -38$ meV, $E_{\text{ad+zp } 1}^{\text{e-v}} = -131$ meV, and $E_{\text{antiad } 1}^{\text{e-v}} = -97$ meV. These estimates should be compared to the exact ground-state energy lowering obtained by exact Lanczos diagonalization: $E_{\text{exact } 1}^{\text{e-v}} = -76$ meV [105]. The better accuracy of the perturbative antiadiabatic estimate is due to the relatively small-to-intermediate value of the total $\sum_k g_k^2 = 0.84$ (Fig. 6.3 indicates that the zero-point corrected adiabatic energy $E_{\text{ad+zp } 1}^{\text{e-v}}$ becomes fairly accurate only beyond $\sum_k g_k^2 \geq 1.5$). For $n = 2$ $S = 0$, and even for $n = 1$ if the larger couplings from PES [93] are taken, the adiabatic estimate comes in much better agreement, especially after a zero-point softening correction is included [105, 106]. In effect, this adiabatic-plus-zero-point-correction approximation should be quite generally applicable to all strongly coupled JT problems. The relative difference of the classical adiabatic energy from the exact energy shows the relative importance of phonon quantum effects in C_{60}^{n-} . So, while for $n = 1$ – a weaker coupling case – the exact energy lies closer to the antiadiabatic expression, the exact result for $n = 3$ and even more for $n = 2$ is much closer to the adiabatic (zero-point corrected) estimate, because in C_{60}^{2-} and C_{60}^{3-} JT coupling is effectively stronger (see Table 6.1).

Even with the uncertainties on the exact value of the couplings, fullerene ions are generally taken as intermediate- to strong-coupled JT systems, the relatively strong coupling realized as the cooperative effect of several moderate individual couplings. This fact is more general: any JT system with a large enough number of vibron modes weakly-coupled to the *same* electronic level behaves as if strongly coupled, since the contributions to the splitting of the electronic multiplet add cooperatively. In fact, for intermediate coupling, the JT energy gains of the individual modes do *not add* algebraically, as they would in the limiting perturbative and adiabatic regimes. To further understand this, we may wish to see the splitting as if effectively due to the coupling to a single mode. In this picture, the addition of more coupled modes effectively acts like an increase in g , thus a rightward shift along the solid line of Fig. 6.3. Since the curvature is upward, the sum of the individual energy

Table 6.3. Perturbative (weak coupling, to order g^2) and semiclassical (strong coupling, to order g^{-2}) electron-phonon pair energies for an H_g mode coupled to an average n electrons in a t_{1u} orbital, assuming for all n a low-spin ground state. The numerical pairing energies are computed for the C_{60}^- couplings of Ref. [70] (see Table 6.2) in the anti-adiabatic approximation. The last column includes the contribution $-\sum g_k^2 \hbar \omega_k = -93$ meV of the A_g modes [107]. The strong-coupling expressions are rigorously valid only in the limit where the intra-shell electron-electron repulsion can be totally neglected.

C_{60}^{n-}	$\mathcal{U}_n^{e-v}/(\hbar\omega)$	$\mathcal{U}_n^{e-v}/(\hbar\omega)$	\mathcal{U}_n^{e-v} [meV]	\mathcal{U}_n^{e-v} [meV]
n	antiadiab	adiabatic	$[H_g \text{ modes only}]$	$[A_g \text{ and } H_g \text{ modes}]$
	$[g \rightarrow 0]$	$[g \rightarrow \infty]$	(antiadiab)	
1	$-\frac{5}{2}g^2$	$-g^2 + 1 - \frac{7}{12}g^{-2}$	-195	-288
2	$5g^2$	$2g^2 - \frac{1}{2} + \frac{13}{24}g^{-2}$	390	297
3	$-\frac{5}{2}g^2$	$-g^2 + 1 - \frac{7}{12}g^{-2}$	-195	-288

gains for each mode coupled separately is always larger than what one obtains from diagonalizing with all the modes included together.

In a solid-state context, electron hopping between molecules will alter this picture as soon as it is large enough to disturb substantially the local JT physics. However, as we will argue later on, the relevant hopping is not so much the bare electron hopping, but rather the quasiparticle effective hopping, a quantity which becomes much smaller near a Mott transition. So long as that effective hopping is small enough, the JT energetics as described above is expected to hold even in the solid state. Electronic correlation in a compound where conduction occurs through electron hopping between C_{60} ionic sites is mainly governed by the extra electron-electron repulsion when the local charge fluctuates away from its average filling of n electrons. The *pair energy*, or Hubbard U , defined by

$$\mathcal{U}_n = E_{n+1} + E_{n-1} - 2E_n, \quad (6.5)$$

(where E_n are the fully relaxed ground-state energies of n electrons) measures precisely the strength of this local correlation. As we shall see in detail below (Sec. 6.2.4), \mathcal{U}_n is largely dominated by the positive Coulomb electron-electron repulsion. However, also the JT electron-phonon energies E_n^{e-v} of Table 6.1 show a strong nonlinear n -dependence, and thus necessarily also contributes to \mathcal{U}_n .

In the standard many-body perturbation theory language, formally \mathcal{U}_n^{e-v} is the real part of the two-electron vertex function at zero frequency, including electron-phonon contributions in the weak-coupling antiadiabatic limit. The contribution of a nondegenerate A_g mode $\mathcal{U}_n^{e-v A_g} \equiv -g^2 \hbar \omega < 0$, independent of n and irrespective of spin S . If coupling to A_g modes prevailed, the electron-phonon pair energy would be negative, and thus electrons would lower their energy if, rather than keeping a uniform occupancy n of all sites, they separated into $(n-1)$ and $(n+1)$ at different molecules, thus creating a bipolaron, or a charge density wave. Even though charge disproportionation has been claimed to play some role in K_3C_{60} [108], in practice the large value of the on-site Coulomb repulsive U parte rules this possibility out in the fullerenes.

Assuming a low-spin ground state for all n (we shall discuss the validity of this assumption in Sec. 6.2.4), Table 6.1 provides all the ingredients necessary to

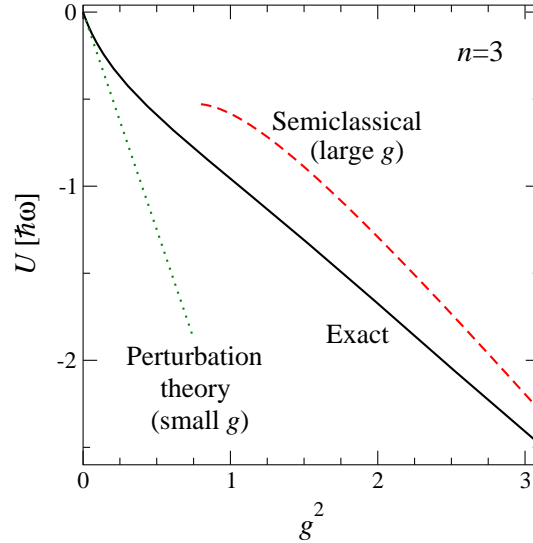


Fig. 6.4. Exact single-mode electron-phonon pair-binding energy \mathcal{U}_1^{e-v} (solid line), compared to weak-coupling perturbation theory for $g \ll 1$ (dotted) and semiclassical theory for $g \gg 1$ (dashed). \mathcal{U}_n^{e-v} is similar for $n = 1, 3, 5$ electrons. The coupling strengths g^2 for the C_{60} modes are all less than ≈ 1 . (Adapted from Ref. [78].)

determine approximate expressions for the H_g modes contribution to \mathcal{U}_n^{e-v} , both in the antiadiabatic limit and in the adiabatic limit (neglecting retardation completely). These expressions are reported in Table 6.3. For odd n , \mathcal{U}_n^{e-v} is *negative*, thus as customary the electron-phonon coupling is attractive and favors pairing [109], thus opposing Coulomb repulsion. Interestingly, for even $n = 2, 4$, \mathcal{U}_n^{e-v} is instead *positive*: here the electron-phonon coupling of the JT type re-enforces the Coulomb repulsion and contributes to *suppress* local fluctuations away from the average number n of electrons at each site. The sign change of the JT contribution to \mathcal{U}_n is due to the nonparabolic dependence of the ground-state energy on n , as reported in Table 6.1. Figure 6.4 shows a comparison of the approximate expressions with the pair energy obtained by exact diagonalization for $n = 3$. As for the total energy, the exact pair energy is bracketed between the antiadiabatic estimate (overestimating) and the semiclassical adiabatic expression (underestimating).

The couplings of Table 6.2 can be plugged into the expressions of Table 6.3, to obtain an estimate of the phonon contributions to the pair energy. In Table 6.3 we use the (probably underestimated) couplings of Ref. [70], and the antiadiabatic approximation (which instead overestimates \mathcal{U}_n), to obtain our best realistic estimate of the phonon contribution to the pair energies. These values are relatively large, and even though they come a long way from reversing the much larger Coulomb repulsion addressed in Sec. 6.2.4 below, they represent a serious correction with cannot be neglected.

6.2.4 Intramolecular Coulomb repulsion and Hund's rule exchange

We come now to the Coulomb electron-electron intra-molecular energetics. As appropriate to an orbitally degenerate level, two distinct Coulomb enter: the ‘‘Hubbard U’’ term coupling to the total charge in the degenerate shell, and an intramolecular exchange term. The first term is strictly related to the pair energy of Eq. (6.5): basically measuring the energy cost required to change electron occupancy of n of the molecular site. In a solid conductor, this term will oppose all local fluctuations away from the average occupancy. Exchange terms, of smaller value, act instead to split multiplets at any given fixed occupancy. They enforce in particular the first two Hund rules, lowering in energy the otherwise degenerate multiplet states of highest spin and largest orbital momentum.

The structure of the Coulomb Hamiltonian for a $(t_{1u})^n$ configuration is formally the same as that for an atomic p^n in spherical symmetry, and as such entirely determined by two parameters only, usually chosen as the configuration-averaged U and a Hund-rule intra-molecular exchange J [72, 110, 111]. For a detailed symmetry analysis of the structure of the Coulomb Hamiltonian \hat{H}^{e-e} , we refer to Ref. [112].

The Coulomb Hamiltonian is a 2-body electronic operator which can be written as

$$\hat{H}^{e-e} = \frac{1}{2} \sum_{\sigma, \sigma'} \sum_{\substack{m, m' \\ n, n'}} w_{\sigma, \sigma'}(m, m'; n, n') \hat{c}_{m\sigma}^\dagger \hat{c}_{m'\sigma'}^\dagger \hat{c}_{n'\sigma'} \hat{c}_{n\sigma}, \quad (6.6)$$

where the Coulomb integrals

$$w_{\sigma, \sigma'}(m, m'; n, n') = \int d^3r \int d^3r' \varphi_{m\sigma}^*(\mathbf{r}) \varphi_{m'\sigma'}^*(\mathbf{r}') u_{\sigma, \sigma'}(\mathbf{r}, \mathbf{r}') \varphi_{n\sigma}(\mathbf{r}) \varphi_{n'\sigma'}(\mathbf{r}') \quad (6.7)$$

are expressed on the basis of the single-particle LUMO wave functions $\varphi_{m\sigma}(\mathbf{r})$, associated to the fermion operators $\hat{c}_{m\sigma}^\dagger$ introduced above.

These Coulomb integrals (6.7) can be evaluated directly for the simple kernel $u_{\sigma, \sigma'}(\mathbf{r}, \mathbf{r}') = q_e^2 / (4\pi\epsilon_0 |\mathbf{r} - \mathbf{r}'|)$, with phenomenological molecular orbitals [113]. This approach neglects the screening due to the other electrons within the same fullerene molecule. Due to that, it yields very large exchange values, close to early Hartree-Fock results [114], which generally overestimate exchange due precisely to lack of screening. With that in mind, one can regard as substantially more realistic the evaluation of the interaction Hamiltonian (6.6) obtained in Ref. [112] on the basis of DFT-LDA electronic structure calculations, which account for the full polarization response of the total charge density. Since on the other hand LDA overestimates screening, the outcome of this calculation represents in turn an underestimate of actual intramolecular exchange.

Like in the atomic case, the symmetry of the Coulomb interaction plus the molecular symmetry of the problem allow us to express all of the Coulomb integrals in (6.7) as functions of a small set of physical parameters. Indeed, the Coulomb integrals are expressed as follows

$$w(m, m'; n, n') = \sum_{\Lambda=A_g, H_g} F^\Lambda \left(\sum_{\mu} C_{mn}^{A\mu} C_{m'n'}^{A\mu} \right) \quad (6.8)$$

in terms of a *minimal* set of independent parameters F^Λ , defined as:

$$F^A = \frac{1}{|A|} \sum_{\mu} \int d^3r \int d^3r' \Phi_{\mu}^A(\mathbf{r}) u(\mathbf{r}, \mathbf{r}') \Phi_{\mu}^A(\mathbf{r}'), \quad (6.9)$$

with

$$\Phi_{\mu}^A(\mathbf{r}) = \sum_{m,n} C_{mn}^{A\mu} \varphi_m(\mathbf{r}) \varphi_n(\mathbf{r}). \quad (6.10)$$

The two parameters governing \hat{H}^{e-e} are related to the $k = 0$ and $k = 2$ Slater-Condon integrals $F^{(k)}$ for p electrons in spherical symmetry [115].

With the decomposition (6.8) in hand, it is convenient to re-organize the interaction Hamiltonian (6.6) in terms of number-conserving symmetry-adapted fermion operators:

$$\hat{H}^{e-e} = \frac{1}{2} \sum_{\Lambda} F^{\Lambda} \left(\sum_{\mu} \hat{w}^{\Lambda\mu} \hat{w}^{\Lambda\mu} \right) - \frac{1}{6} \left(F^{A_g} - 5F^{H_g} \right) \hat{n} \quad (6.11)$$

where we defined the operators

$$\hat{w}^{\Lambda\mu} := \sum_{\sigma} \sum_{mn} C_{mn}^{A\mu} \hat{c}_{m\sigma}^{\dagger} \hat{c}_{n\sigma}. \quad (6.12)$$

Rather than the F^A parameters, it is customary to use the parameters $U = F^{A_g}/3 - F^{H_g}/3$, and $J = F^{H_g}/2$ (the notation K is sometimes used for this quantity; it also equals $F^{(2)}/3$ of spherical symmetry [72, 115]). With this definition, observe that

$$E^{e-e \text{ ave}}(n) = \text{Tr}|_n(\hat{H}^{e-e}) = U \frac{n(n-1)}{2}, \quad (6.13)$$

where $\text{Tr}|_n$ is the trace restricted to the n -electrons states. U governs therefore the parabolic dependence of the Coulomb energy averaged over all possible multiplet configurations on the total number of electrons n . It should be noted that U involves average multiplet energies, not *ground-state energies* like the pair binding energy of Eq. (6.5): the two quantities therefore would only coincide in a hypothetical system where multiplets were unsplit by JT and exchange terms. With standard multiplet splitting instead, the pair-energy definition, based on the ground-state energy, depends on n , which makes it rather inconvenient to characterize the Coulomb repulsion in the t_{1u} shell with a single microscopical parameter.

The J parameter controls the multiplet exchange splittings, i.e. it implements Hund's rules. One can label all multiplet states with an orbital "angular momentum" L (recall that the t_{1u} orbitals behave effectively as p orbitals), as in Table 6.4. In fact, it is possible to express the Coulomb energy of all multiplets with the equation

$$E^{e-e}(n, S, L) = U \frac{n(n-1)}{2} - J \left[2S(S+1) + \frac{1}{2}L(L+1) + \frac{1}{2}n(n-6) \right], \quad (6.14)$$

as a function of n , S and L [112]. These energies are also reported in Table 6.4.

The Coulomb parameters were computed by ab-initio density-functional calculations in Ref. [112]. The value of the molecular Hubbard U term of isolated C_{60} was determined $U = 3.07$ eV, in the same range as previous calculations [110, 116, 117, 118]. This estimate can be compared to experiment. The pair energy $\mathcal{U}_1 = E_0 + E_2 - 2E_1 = (E_0 - E_1) - (E_1 - E_2) = E_A(C_{60}) - E_A(C_{60}^-)$, where E_A indicates the electron affinity. These quantities are experimentally available for molecular C_{60} [40] and C_{60}^- [43, 119]

Table 6.4. Coulomb energies for the $(t_{1u})^n$ or p^n multiplets expressed in terms of the two Coulomb parameters U and J . These multiplets are correct under the assumption that electron-phonon coupling can be totally neglected. The $n = 4$ and $n = 5$ multiplet have the same J terms as $n = 2$ and $n = 1$, with the center-of-mass (U) term given by Eq. (6.13): $6U$ and $10U$ respectively.

C_{60}^{n-}	$(2S+1)[L]$	$(2S+1)\lambda$	$E^{e-e}(n, S, L)$
1	2P	$^2t_{1u}$	0
2	1S	1a_g	$U + 4J$
2	1D	1h_g	$U + J$
2	3P	$^3t_{1g}$	$U - J$
3	2P	$^2t_{1u}$	$3U + 2J$
3	2D	2h_u	$3U$
3	4S	4a_u	$3U - 3J$

Table 6.5. The energy (in meV) of the lowest state of t_{1u}^n for each n and S , including the electron-electron and JT contributions from $\hat{H}_0 + \hat{H}_{e-v} + \hat{H}^{e-e}$ (but excluding the $[en + Un(n-1)/2]$ term). Adiabatic approximation: the phonons are treated in the adiabatic (strong-coupling) approximation, by full relaxation of the phonon modes to the optimal classical JT distortion for each n and S . Anti-adiabatic: the electron-phonon behaves effectively as a negative $J^{e-v} = -\frac{3}{4} \sum_k g_k^2 \hbar \omega_k$ [112]: the combined Hund and JT interaction yields levels split according to the pattern of Table 6.4, with J replaced by $J + J^{e-v}$. (From Ref. [112].)

n	S	adiabatic	anti-adiabatic
2	0	-92	-100
	1	-71	-25
3	1/2	-85	-50
	3/2	-97	+75

$$E_A(C_{60}) - E_A(C_{60}^-) = 2.7 \text{ eV} - 0.17 \text{ eV} \approx 2.5 \text{ eV}. \quad (6.15)$$

This value is slightly reduced from pure Coulomb by electron-phonon coupling and orbital relaxation (see also Table 6.3). If we neglect these comparatively small contributions to the pair energy $\mathcal{U}_1 \approx U$: a range $U \simeq 2.5 \div 3$ eV provides a realistic estimate of the actual U parameter of gas-phase C_{60} .

For the intra-orbital exchange interaction, the calculation of Ref. [112] finds a value $J = 32$ meV. Calculations where screening is ignored or underestimated find much larger values, e.g. $J = 110$ meV (Hartree-Fock [114]) and $J = 95$ meV (calculation of the unscreened integrals in model orbitals [113]). An early calculation including screening by the strongly polarizable C_{60} molecule found $J = 25$ meV [110]. Because DFT tends to overestimate screening, DFT values of J may be somewhat underestimated. We believe that the actual Coulomb parameters of C_{60} could lie somewhere in between the DFT couplings assumed here and the “bare” ones of Ref. [113, 120], but most likely closer to the DFT ones, due to the large polarizability of C_{60} . An intermediate value of $J \simeq 50$ meV is probably realistic.

It should be noted in this respect that suggestions advanced in earlier times that overscreening could reverse altogether the sign of this frozen-molecule, purely electronic exchange J [109, 121, 122] appear incorrect. This is confirmed by recent purely electronic quantum Monte Carlo calculations [123] finding a spin gap between triplet (ground) and singlet (excited) states consistent with $J \simeq 54$ meV. What is emerging as the correct picture is that only after inclusion of nuclear motion, and specifically of JT effects that are strongly anti-exchange, the *effective* J may change sign, from positive to negative. As the above results in fact show, the JT energetics is opposed to Hund's rule, and favor low-spin states against intra-molecular exchange, as evident from Table 6.1. The effects of the two interactions, electronic exchange and JT, tend to cancel. In fact the antiadiabatic expressions of the JT energies (Table 6.1 and Ref. [23]) are consistent with the structure given by Eq. (6.14), if we replace J with a negative local exchange $J^{e-v} = -\frac{3}{4} \sum_k g_k^2 \hbar \omega_k$. Therefore when the antiadiabatic approximation holds – for example when the JT coupling is weak and the effective electron hopping is much smaller than important H_g vibration frequencies – one can account simultaneously for both JT and Coulomb exchange by replacing J with an effective $J_{\text{eff}} = J + J^{e-v}$. The resulting energetics for C_{60}^{n-} ions is summarized in Table 6.5. Likewise, an additional term $J^{e-v} \frac{1}{3} n(6-n)$ must be introduced to account for the shift of the center of mass and contributes $U^{e-v} = \frac{2}{3} J^{e-v} = -\frac{1}{2} \sum_k g_k^2 \hbar \omega_k$ to the multiplet center-mass Coulomb U . However, as $U \gg J$, the cancellation of U is much less effective than for the exchange term, and the phonon's contribution leaves a strongly repulsive total U . We should stress again that for general couplings and general electron hoppings the electron-vibration and electron-electron contributions do not add so simply, and must be treated in full [124, 125]. Nevertheless these approximate results are quite useful in providing a basic insight in this competition.

The balance between Hund's rule exchange and JT is much less definite for C_{60}^{n+} , where, according to calculations [105], overall Coulomb exchange marginally prevails, leading to regular Hund's rule high-spin ground states. In that case, for example C_{60}^{n+} should have a $S = 1$ ground state as an isolated ion, and might or might not retain high spin in solution [59] or in solid-state compounds [61, 62, 63, 64], depending on the environment.

Experiments do confirm a substantial screening of J . Consider first C_{60}^{4-} , present in insulating A_4C_{60} ($A=K, Rb$). NMR [126, 127, 128] has identified an important singlet-triplet excitation around $100 \div 140$ meV. Taking this spin gap as representative of the $^1S \rightarrow ^3P$ transition between the singlet molecular ground state and the lowest triplet state (separated by $5 J_{\text{eff}}$ according to Table 6.4), NMR data are consistent with a small effective value of $J_{\text{eff}} \simeq -20 \div -28$ meV. Thus the electron-phonon coupling counteracts very effectively the Hund's rule exchange, and eventually prevails, even if marginally, in these electron-doped fullerene compounds. As we will see below, this is the origin of the low-spin character of the Mott insulating phases (Mott JT insulators), and of (singlet, s-wave) superconductivity in fullerenes. EPR and NMR of discrete salts indicate that also C_{60}^{3-} ions have a low-spin ground state [129, 130]. The case of C_{60}^{2-} is more intriguing. Here, it appears that the balance between Coulomb effects, matrix effects, and JT energies is more critical, and the final ground state can jump between 3P and 1S , depending on marginal effects. Early reports suggested that when frozen in an organic glass, C_{60}^{2-} is in a triplet state [44], but this evidence has been questioned [15]. In discrete salts, the singlet and triplet have been claimed to coincide closely [131, 132], whereas in solutions

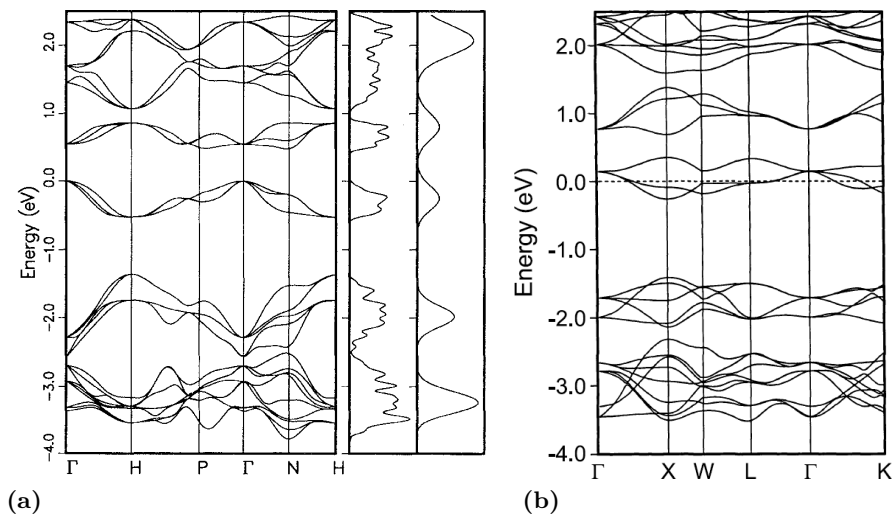


Fig. 6.5. (a) Band structure of K_6C_{60} . Energy is referred to the t_{1u} band maximum. The solid-state density of states is compared to Gaussian-broadened single-molecule levels. (From Ref. [139].) (b) Band structure of K_3C_{60} . Energy is referred to the Fermi level. (From Ref. [1].)

the singlet appears to be stabilized by about 70 meV [15, 133, 134]. Evidence of a 10 meV spin gap attributed to long-lived fluctuating C_{60}^{2-} in cubic CsC_{60} suggests almost complete compensation, with marginal prevalence of the singlet state [135]. On the other hand, ferromagnetism of TDAE- C_{60} [136] has been interpreted [137] in terms of fluctuating $S = 1$ local C_{60}^{2-} sites. Structural evidence of a JT distortion is relatively rare. When available it is not especially clear in showing twice larger distortion in C_{60}^{2-} [138] relative to C_{60}^- , which is what is expected for low spin. The only indirect evidence of a distortion in K_4C_{60} is provided by the splitting of the highest T_{1u} vibrational mode demonstrated in Ref. [7].

In summary, experimental and theoretical evidence agrees that (i) in the energy comparison between different number occupancies n (pair energy U_n) the repulsive Coulomb energies dominate; (ii) in the energy comparison between different multiplet (spin) states at fixed occupancy n (exchange term J), the attractive anti-Hund JT energies tends to prevail over slightly weaker competing Coulomb exchange, but there are exceptions and high spin may prevail in particular environments.

6.3 Strong correlation in solid alkali fullerenes: general

After this long preliminary on the properties of molecular ions we now come to the solid state compounds, that constitute our main concern. The starting point for the discussion of their electronic behavior is as always the standard electron band structure. The band structure of solid alkali fullerenes has been computed by many authors [1, 3, 139, 140, 141], generally based on DFT-LDA methods. As illustrated in Figs. 6.5 and 6.6, the bandwidth W of the LUMO band is generally obtained in

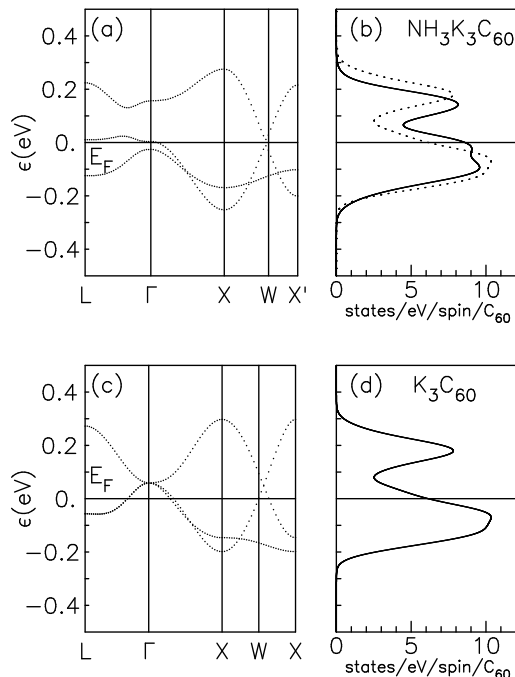


Fig. 6.6. LUMO band structure of $\text{NH}_3\text{K}_3\text{C}_{60}$ (a), obtained by an DFT-LDA calculation, compared to that of K_3C_{60} (c). The corresponding densities of states are given in panels (b) and (d). In panel (b) the density of states of K_3C_{60} (dashed line) is re-drawn for direct comparison with that of $\text{NH}_3\text{K}_3\text{C}_{60}$ (solid line). (From Ref. [140].)

the 500 ÷ 600 meV region. Differences for different lattice structures are of course present, as well as a strong dependence upon the relative rotational ordering of the C_{60} balls [142]. In particular, smaller bandwidths are obtained in correspondence of larger lattice spacings, associated, e.g., to larger intercalated cations such as Cs^+ in the place of K^+ . The main observation is that the electron bandwidths in the solid are generally a fraction of the separation between neighboring molecular levels, the latter giving rise to well defined rigid bands. In particular, the threefold LUMO band remains well separated from the LUMO+1 and HOMO bands through the Brillouin zone. The metal-insulator transition in the C_{60}^{n-} -based compounds can then be interpreted in terms of the localization of the electrons within the partly filled t_{1u} LUMO band. Self-energy effects are predicted to increase W by about 30% in the usually more accurate GW approximation over that calculated by LDA [142].

A direct experimental determination of the bands in solid C_{60} compounds is complicated by characteristic strong electron-phonon satellites derived from the vibronic couplings of Sec. 6.2.3, which tend to broaden and influence all spectra. Angle-resolved photoemission, which could access directly the band dispersion is made additionally hard by the orientational disorder and the small size of the Brillouin zone. A recent experiment [143] accessed directly the dispersion in a K_3C_{60}

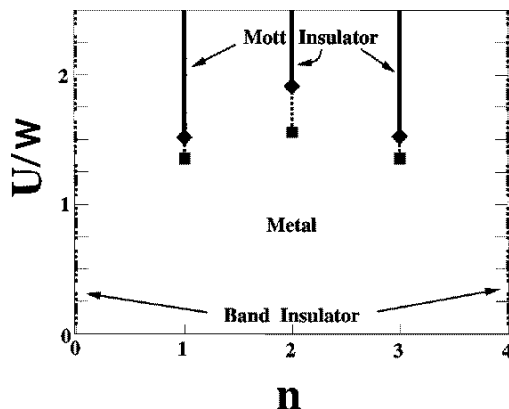


Fig. 6.7. DMFT zero-temperature phase diagram for the two-band Hubbard model as a function of filling and of the ratio U/W of the local Coulomb repulsion to the half width. In this calculation molecular Coulomb exchange $J = 0$, and the possibilities of magnetism and/or charge order are ignored. The $T = 0$ Mott transitions at integer filling are located between the pairs of finite-temperature estimates indicated by squares and diamonds. (Adapted from Ref. [152].)

monolayer, obtaining an estimate $W \approx 250$ meV, significantly smaller than the DFT-LDA bandwidth of the monolayer. Newer experiments on K_3C_{60} multilayers find an even smaller $W \approx 150$ meV, about one third of the DFT bandwidth [144]. These small values do not deny the DFT estimates but most likely represent a quasiparticle effective dispersion, whose magnitude relative to the bare band dispersion is strongly affected, and nontrivially reduced by correlations. It should be noted that, even if there is so far no accurate prediction for the full \mathbf{k} -dependent spectral function, this kind of observed electron dispersion is not to be identified with the simple quasiparticle bandwidth zW either. The effective observed bandwidth probably corresponds to the intermediate energy scale discussed in recent DMFT studies of a simplified model, where it is designated as T_+ [145, 146, 147]. Indeed, the same angle-resolved photoemission measurement carried out on K_6C_{60} , where correlations play no role, find [144] a band dispersion in very good quantitative agreement with the DFT calculation of Fig. 6.5 ($W \simeq 0.6$ eV) [139].

In the light of the discussion of Sec. 6.2.4, it is clear that the largest energy scale of for the LUMO-band electrons in the fullerenes is the Coulomb repulsion U . It remains the largest energy scale, even with the extra screening characteristic of the solid state, which appears to reduce the molecular U from about $2.5 \div 3$ eV to a smaller $0.9 \div 1.6$ eV [116, 148, 149, 150, 151]. The smallest value in this range is probably closer to the correct bulk estimate in the metallic doped materials, while the upper value better characterizes insulating states and the molecules at the surface, where screening may be less effective due to reduced coordination [16, 116]. The ratio of the local Coulomb repulsion to the bandwidth can therefore be estimated in the range $1.5 \leq U/W \leq 3$ for typical LUMO-band electrons in standard fullerenes.

A local Coulomb repulsion larger than the bandwidth is the signature of strong electron correlation in a solid. Situations of this kind are conventionally described

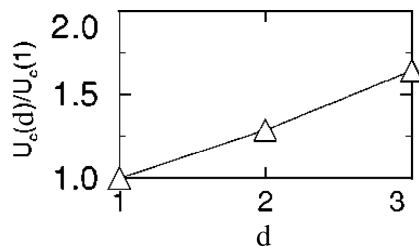


Fig. 6.8. The critical U_c/W as a function of orbital degeneracy d at half filling $n = d$. For $d = 1$ band $U_c^{1\text{-band}} \approx 1.46W$. In these DMFT calculations the local Coulomb exchange is neglected ($J = 0$). The possibility of magnetic and/or charge and/or superconductive order is also ignored. (Adapted from Ref. [154].)

in the language of Hubbard models. The single-band half-filled 3D Hubbard model is believed to undergo a metal-insulator transition of the Mott type, as soon as the ratio U/W exceeds some critical U_c/W of order unity [153]. The conventional small- U metal transforms to a large- U Mott-insulator where electrons remain essentially frozen, one at each site, so that the occurrence of zero and double occupancies is strongly even if not totally suppressed. The residual effect of intersite hopping is to induce a generally antiferromagnetic correlation between the spins of electron at neighboring sites. Away from half filling the model has a metallic (and possibly superconducting) ground state even for large U/W .

The single-band Hubbard model, however, can hardly be applied to the fullerenes, where there are $d = 3$ relevant bands, derived from the three degenerate molecular LUMO orbitals. The rough physics of the multi-band Hubbard model is summarized in the phase diagram of Fig. 6.7, for the simpler case of only $d = 2$ bands. At integer-filling, lines of strongly correlated Mott insulators extending above U_c/W are surrounded by the metallic phase encompassing all noninteger fillings. The same qualitative picture should hold for $d = 3$, where metal-insulator transitions should occur for stoichiometric phases, in particular $n = 3$ (as in K_3C_{60}) and $n = 4$ (as in K_4C_{60}).

Recently, the metal-insulator transition has been attacked theoretically within the dynamical mean field theory (DMFT) [155]. This method, which becomes exact in the limit of large space dimensions, has provided quantitative estimates of the U_c/W under various conditions. The lines of Fig. 6.7 are constructed based on the DMFT [152], assuming a “pure” Mott transition, with no complications induced by possible spin or/and charge order in the insulating phase. The “paramagnetic” Mott-Hubbard transition occurs at different critical U for different orbital degeneracy d (number of bands) and fillings n . Earlier work showed that the Mott transition in orbitally d -degenerate lattice models takes place at larger values U_c/W for larger degeneracy d , roughly proportionally to \sqrt{d} [156, 154, 157], as illustrated in Fig. 6.8. Specifically, the Mott transition in the half-filled one-band model ($d = 1$, $n = 1$) has been calculated at $U_c^{1\text{-band}}/W \approx 1.3$ in a previous DMFT study based on the the quantum Monte Carlo method at the relatively low temperature $T = W/32$ [158]. A more accurate $T = 0$ estimate of $U_c^{1\text{-band}}/W \approx 1.46$ is provided by iterated perturbation theory [155]. The transition was found at $U_c^{2\text{-band}}/W \approx 1.5$ for $d = 2$, $n=1$ [152], and $U_c^{2\text{-band}}/W \approx 1.8$ for $d = 2$, $n=2$ [152, 154], with the same method,

and at the same temperature. $T = 0$ Lanczos diagonalization DMFT calculations push these values slightly up, with the $n=1$ value close to $U_c^{2\text{-band}}/W \approx 1.8$ [140]. For $d = 3, n=3$, the transition was located close to $U_c^{3\text{-band}}/W \approx 2.3$ [154], although at a slightly higher temperature. The finite temperature appears to affect somewhat the numerical values: the zero-temperature DMFT calculations based on Lanczos diagonalization provide slightly larger values [159], but confirm that $U_c^{3\text{-band}} > U_c^{2\text{-band}} > U_c^{1\text{-band}}$ [140].

These values of U_c/W are significantly reduced when more realistic DMFT calculations allow for intra-site couplings and the ensuing magnetically/charge ordered phases, and when any kind of local exchange term is included to break the local multiplet degeneracy. Therefore one cannot compare directly the values of U_c/W from paramagnetic DMFT calculations of the multi-band Hubbard model with the metal-insulator transition in the actual compound, where it is affected by the detailed band structure, nesting, JT electron-vibration interaction and intra-site exchange. Most of these effects tend to lower U_c .

In fact, the range $1.5 \leq U/W \leq 3$ typical of the alkali fullerenes should put all these materials above the metal-insulator transition: all integer-filled compounds should then be insulators. In practice, the alkali fullerenes lie experimentally close to the Mott transition, on both sides. Different compounds exhibit a variety of behavior, including unconventional metals like cubic CsC_{60} [135], superconductors of the A_3C_{60} family (A= K,Rb,Cs) [13, 151] including also $\text{NH}_3\text{Na}_2\text{CsC}_{60}$ [160], a ferromagnet – TDAE- C_{60} [50, 51, 136, 137, 161, 162], and Mott insulators. Among the latter we can place A_4C_{60} [4], possibly Na_2C_{60} [163], $(\text{NH}_3)_6\text{Li}_3\text{C}_{60}$ [12], and the full class of compounds $\text{NH}_3\text{K}_3\text{C}_{60}$, $\text{NH}_3\text{K}_2\text{RbC}_{60}$, $\text{NH}_3\text{KRb}_2\text{C}_{60}$, and $\text{NH}_3\text{Rb}_3\text{C}_{60}$ [6, 8, 9]. The fact that the $n = 2, 4$ compounds are insulators is not especially surprising in view of the increase in repulsive pair energy due to electron-phonon contribution (Sec. 6.2.3), and the probably smaller $U_c^{3\text{-band}}(n = 2) < U_c^{3\text{-band}}(n = 3)$. Altogether, this scenario indicates a reduction of U in solid fullerenes, and a lowering of U_c relative to its bare theoretical value of Figs. 6.7 and 6.8.

Magnetic susceptibility data [12, 164] in particular place the metallic/superconducting C_{60}^{3-} compounds close to the metal-insulator transition. Indeed, in the Hubbard model, the strongly-correlated metallic state near U_c is expected to show an anomalously large uniform magnetic susceptibility χ compared to the free-electron value $\mu_B^2 N(\epsilon_F)$ (where $N(\epsilon_F)$ is the density of states per C_{60} at the Fermi energy ϵ_F) [155]. The magnetic susceptibility is observed to increase rapidly with the lattice spacing in the C_{60}^{3-} fullerenes [12, 164]. When moving closer to the metal-insulator transition, the observed increase cannot be interpreted purely in terms of band narrowing and a related increase in the density of states at the Fermi level $N(\epsilon_F)$. The discrepancy between this increase due to bare band narrowing and observation is huge, and can only be explained by strong correlations.

Further, if less direct, evidence of the strong electronic correlation in K_3C_{60} is provided by the electron spectral function at E_F which can be assimilated to a narrow, dispersionless Kondo-like resonance by photoemission data [165]. On the other hand, photoemission is on one hand strongly affected by vibrational effects and also possibly more sensitive to surface molecules [166], where correlation is stronger due to a less screened Hubbard U , thus caution is required before photoemission data should be taken as representative of bulk K_3C_{60} as magnetic susceptibility data can.

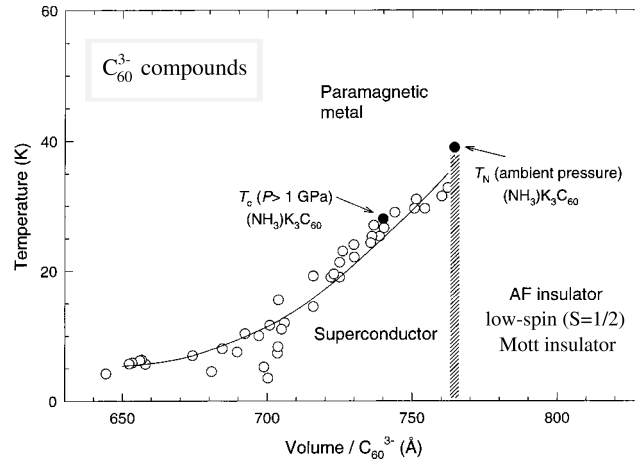


Fig. 6.9. Schematic electronic phase diagram of C_{60}^{3-} compounds, showing the approximate location of the metal (superconductor)-insulator phase boundary. The open symbols are literature values of T_c for a variety of superconducting fullerenes, while the solid symbols mark T_N (ambient pressure) and T_c (> 1 GPa) of $NH_3 K_3 C_{60}$. This expanded trivalent fullerene is only metallic and superconducting under pressure, and reverts to an antiferromagnetic insulator at zero pressure, in strong analogy with the cuprates (exchanging pressure with doping). Moreover, the C_{60}^{3-} is in a $S = 1/2$, low-spin state, and not in $S = 3/2$ high-spin state. This indicates an effective inversion of the effective Hund's rule J , supporting the conclusion that $NH_3 K_3 C_{60}$ and related compounds are Mott-JT insulators. (Adapted from Ref. [167].)

In the ammoniated compounds, insertion of the electronically inert NH_3 molecules expands the C_{60} lattice, turning the cubic, metallic, and superconducting state of $K_3 C_{60}$ into an orthorhombic narrow-gap $S = 1/2$ antiferromagnetic insulator [6, 8, 168]. Upon application of pressure to $NH_3 K_3 C_{60}$, the Mott insulating state reverts to a fully metallic and superconducting – while still orthorhombic – phase [169, 170]. A similar pressure-induced reversion from insulator to metal has been observed in tetragonal $Rb_4 C_{60}$ [126]: these experiments rule out the possibility that metallic states of the fullerenes should entirely be attributed to nonstoichiometry. These transitions in the alkali fullerenes are rare examples of experimentally accessible Mott transitions. We will take that of $NH_3 K_3 C_{60}$ as a paradigm where several of the concepts illustrated above emerge most clearly. It was suggested [167] that the increase in volume per C_{60} molecule relative to $K_3 C_{60}$, with its probable slight decrease of electronic effective bandwidth W , should drive the Mott transition (Fig. 6.9).

While the above is certainly relevant, in addition to the simple change in volume, thus of W , a role of the crystal-structure anisotropy in this pressure-driven transition from the insulator to the metal and superconductor has been proposed [8]. Crystal anisotropy affects hopping between neighboring fullerene balls, making it different for pairs of molecules at different distances, along different crystal directions, thus affecting the band structure. The effect of anisotropy is most clearly seen in the the

band splitting at Γ , illustrated in Fig. 6.6. A strong enough “crystal-field” splitting of the threefold degenerate t_{1u} molecular orbital of C_{60} caused by orthorhombic lattice anisotropy could remove one or several bands away from the Fermi level, effectively reducing the orbital degeneracy d , and shifting the Mott transition to a smaller critical value U_c/W . Exploring this concept, the basic question is how large a splitting is required to promote the effective reduction of degeneracy. In a non-interacting system, that reduction would clearly require a splitting magnitude at least similar to the electron bandwidth W . In a strongly-interacting system, it is important to understand whether the effective degeneracy lifting, and the associated substantial displacement of the metal-insulator transition, will again require anisotropic splittings as large as the bandwidth, or else if some smaller energy scale will emerge in its place.

In the final sections in this chapter we will address this issue within DMFT, by studying the effects of a band splitting on the Mott transition of an orbitally degenerate, strongly correlated metal. The theory for the distorted ammoniated compounds underscores the central role of a new low-energy scale characteristic of strongly correlated itinerant electrons close to the Mott transition: the width zW of the Kondo peak. We will argue about the importance of this concept in the context of both C_{60}^{3-} and C_{60}^{4-} fullerides, and of strongly correlated materials in general.

6.4 Strong correlations in fullerides: theoretical models

Models of alkali fullerides should be able to describe metals, Mott insulators, and superconductors. The largest energy parameter being the intra-molecular repulsion U , with the electron hopping only second, ab initio approaches are not yet in adequate shape to meet this challenge at the present date.

Early work attempted to interpret the superconductivity of the fullerides in terms of Migdal-Eliashberg theory [22, 23, 88, 89, 171, 172, 173, 174, 175, 90]. The necessity to introduce a comparably large value of the pseudopotential $\mu^* \approx 0.4$ already suggests that electronic correlations are exceedingly important. The large zero-point vibrational energy $\frac{1}{2}\hbar\omega$ associated to the vibrationally-derived optical modes of these solids also suggests a breakdown of Migdal’s approximation, and that vertex corrections and other nonadiabatic effects could play a relevant role in the fullerides [176, 177, 178, 179, 180, 181]. However, this kind of theory starts from free electrons in a regular band metals, hard to accept for the fullerides whose large value of U puts them close to (if not beyond) the Mott-Hubbard transition. As anticipated above, for a satisfactory description of the large local Coulomb correlation and of the band physics on the same footing, a multi-band Hubbard model, possibly including the JT phonons, and described within the DMFT [155] or some of its several evolutions [182, 183, 184] is certainly a more natural choice.

The simplest d -band Hubbard model is written as

$$\hat{H} = \hat{H}_{\text{hop}} + \hat{H}^{e-e}. \quad (6.16)$$

Here we assume purely diagonal hoppings between orbitals at nearest neighbor sites i and j :

$$\hat{H}_{\text{hop}} = -t \sum_{\langle i,j \rangle, \sigma} \sum_{m=1}^d \left(\hat{c}_{im\sigma}^\dagger \hat{c}_{jm\sigma} + H.c. \right) + \sum_{i m} \epsilon_m \hat{n}_{im}, \quad (6.17)$$

with d bands of the same width W , the anisotropic symmetry lowering entirely embodied in a local diagonal term splitting the on-site orbital energy ϵ_m . Of course, these simplifying assumption are not strictly applicable to the fullerenes, where a more complicated 3×3 matrix of overlaps for the t_{1u} LUMO orbitals at neighboring sites (possibly including merohedral disorder) should be (and has been) employed [16, 185]. The essence of the Mott transition in the fullerenes should most likely not be affected qualitatively by the details of the hoppings, but the quantitative provisions of a model ignoring the correct tight-binding hopping matrix, including effects of orientational order or merohedral disorder, should not be taken too literally.

The Coulomb part $\hat{H}^{e-e} = \sum_i \hat{H}_{e-e}^i$, with the local term defined in Eq. (6.11) for $d = 3$. Another equivalent formulation for the local term goes as follows:

$$\begin{aligned} \hat{H}_i^{e-e} = & (U + J) \sum_m \hat{n}_{im\uparrow} \hat{n}_{im\downarrow} + (U - J) \sum_{m < m' \sigma} \hat{n}_{im\sigma} \hat{n}_{im'\sigma} \\ & + U \sum_{m \neq m'} \hat{n}_{im\uparrow} \hat{n}_{im'\downarrow} + J \sum_{m \neq m'} \hat{c}_{im'\uparrow}^\dagger \hat{c}_{im\downarrow}^\dagger \hat{c}_{im'\downarrow} \hat{c}_{im\uparrow}, \end{aligned} \quad (6.18)$$

with the advantage that it applies equally well for any degeneracy $d = 1, 2, 3$ [154].

The on-site electron-vibration couplings Eq. (6.4) and the ensuing JT effect, are quite important for many aspects, including superconductivity and resistivity [16, 23, 151, 186], as discussed in Sec. 6.4.4 below. While we included it in the single-ion model of Eq. (6.16), the initial simplification of neglecting the JT coupling in the solid is useful for a simple approach to the basic physics of the Mott transition.

6.4.1 The bare $d = 2$ model with anisotropy

For an initial study of the anisotropy effect on the Mott transition, one can start with the simplest orbitally degenerate Hubbard model, namely $d = 2$ bands, zero JT coupling, zero Hund's rule exchange. For the anisotropy term we can assume, without loss of generality, $\epsilon_2 = -\epsilon_1 = \Delta/2$. We choose to study filling $n = 1$ electron/site: this choice is motivated by the observation that for $d = 2$, half filling $n = d = 2$ would yield a trivial phase diagram, not comparable to the realistic case $n = d = 3$. We study this model at zero temperature, where the Mott transition appears most clearly, as a function of Δ/W and U/W .

In the $U = 0$ limit, the splitting $\Delta > 0$ simply shifts band 2 upwards with respect to band 1, promoting electron transfer from the upper to the lower band. Above a critical value $\Delta = \Delta_c$, the upper band will be emptied. For example, with two symmetric bands, above $\Delta_c/W = 0.5$ the upper band is emptied and the lower band remains half filled. At $U = 0$, the transition between the ‘‘two-band metal’’ and ‘‘one-band metal’’ is continuous. Because the topology of the Fermi surface changes, this transition is accompanied by a weak zero-temperature singularity of the total energy first described by Lifshitz [187]. When the electron-electron interaction U is turned on, one expects the emptying of the upper band to take place at smaller values of Δ_c , owing to the effective band narrowing. Perturbatively in U one can show that at weak coupling

$$\Delta_c(U) = \Delta_c(0) - \gamma U + O(U^2), \quad (6.19)$$

where the value of the coefficient $\gamma > 0$ depends on details of the bands. In addition, electron-electron interactions might modify the nature of the metal-metal transition

singularity relative to the noninteracting case [188], a point which we will not further address here.

The $\Delta = 0$ and $\Delta \rightarrow \infty$ limits reduce then, respectively, to the (quarter-filled) two-band and (half-filled) single-band Hubbard models, both possessing a metal-insulator transition as a function of U [152, 158, 159, 189]. We are not interested here in the weak-coupling antiferromagnetic instability of the ensuing large- Δ half-filled band, associated with the possible presence or absence of nesting characteristic of a specific assumed intersite hopping scheme. Consistently with our neglect of all intrasite multiplet interactions, we also ignore for the moment the possibility of charge ordered and/or superconducting phases. In particular, we leave the local exchange term out ($J = 0$), with the proviso that this term will later be crucial in order to understand the ordered phases which enrich the phase diagram of the model [146, 186, 190, 191]. We assume a genuine Mott transition for the half-filled single-band model to occur at a finite $U_c^{1\text{-band}} > 0$ (for $\Delta \rightarrow \infty$) and $U_c^{2\text{-band}} > U_c^{1\text{-band}}$ (for $\Delta = 0$).

The limit of strong interaction, $U \gg W$, is insulating for any value of Δ . This limit can be studied by mapping the model (6.16) onto a spin and orbital exchange Hamiltonian which reads [137]

$$H_{\text{exch}} = J_t \sum_{\langle i,j \rangle} (\mathbf{S}_i \cdot \mathbf{S}_j + \mathbf{T}_i \cdot \mathbf{T}_j + 4 \mathbf{S}_i \cdot \mathbf{S}_j \mathbf{T}_i \cdot \mathbf{T}_j) - \Delta \sum_i T_i^z, \quad (6.20)$$

where the true spin operator is $\mathbf{S}_j = \frac{1}{2} \sum_{m\nu\nu'} c_{jm\nu}^\dagger \boldsymbol{\sigma}_{\nu\nu'} c_{jm\nu'}$ and the pseudospin-1/2 vector operators $\mathbf{T}_j = \frac{1}{2} \sum_{mm'\nu} c_{jm\nu}^\dagger \boldsymbol{\sigma}_{mm'} c_{jm'\nu}$ represent the orbital degrees of freedom, $\boldsymbol{\sigma}$ being the vector of Pauli matrices, and $J_t = 2t^2/U$. For $\Delta = 0$ this model has been studied both in one [192] and two dimensions [193], with suggestions that interesting spin-liquid physics could be realized. For our purposes, it suffices to note that this model has no ferro-orbital instability, and has therefore a finite $q = 0$ orbital susceptibility. As a consequence it takes a nonzero value of Δ to fully orbitally polarize the ground state. Due to the absence of cross-band terms in the kinetic energy, complete orbital polarization occurs at a finite $\Delta_c \propto J_t = 2t^2/U$. For $\Delta \geq \Delta_c$ the ground state is thus represented by a one-band Mott insulator plus a totally empty split-off band.

For the specific case we are interested in ($n = 1$ electron in a two-fold degenerate band) no orbital ordering is present at weak coupling. On the other hand, the possibility of antiferro-orbital and/or spin ordering within the Mott insulating phase, and of spin-orbital density waves in the intermediate U regime, depends crucially on the details of the various hopping matrix elements and of lattice coordination. These are left out of the infinite-dimensional lattice assumed in the calculations to be described in the following section. Therefore, within the standard scheme of single-site DMFT calculations, we can study the phase diagram of this model restricted to spin and orbital paramagnetic states.

Figure 6.10 is a sketch of the zero-temperature phase diagram of the $d = 2$ model in Eq. (6.16) as a function of (U, Δ) for $n = 1$ electron per site. The transitions at $\Delta = 0$ and $\Delta = \infty$ are located at the values of $U/W \simeq 1.8$ and 1.5 as discussed in Sec. 6.3. The descending AB line in Fig. 6.10, representing U_c as a function of Δ separating metals from Mott insulators, indicating that $U_c^{2\text{-band}} > U_c^{1\text{-band}}$. The DM' line separates the fully orbitally polarized Mott insulator (on the right) from the two-band insulator, roughly as $U_c \sim \Delta^{-1}$ for small Δ . Similarly, the CM

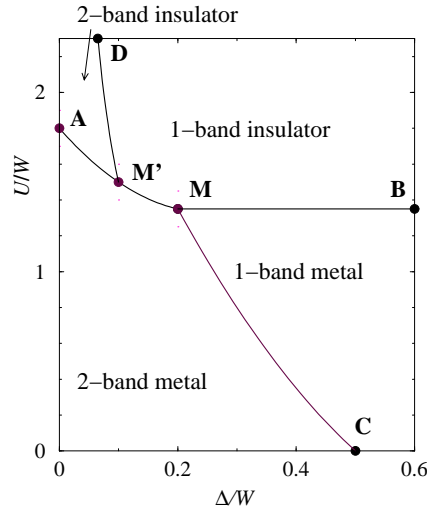


Fig. 6.10. Qualitative zero-temperature phase diagram for the two-band Hubbard model at quarter filling (one electron per site) in the U - Δ plane, where Δ is the anisotropy splitting of the two orbitals. The various phases and lines are described in the text. The multicritical points M and M' are not necessarily distinct. (From Ref. [140].)

line separates the fully orbitally polarized metal from the two-band metal: it starts from point C with a linear slope $-\gamma^{-1}$, according to Eq. (6.19). In the region of full orbital polarization the value of Δ is irrelevant, and this is the reason why the Mott-transition line MB is horizontal. As Δ increases, for $U < U_c^{1\text{-band}}$ the upper-band emptying transition takes the two-band metal across the CM line over to a one-band metal, while for $U > U_c^{1\text{-band}}$ it leads across the AM line to a Mott insulating state. The steeply dropping AM line is the main outcome of the calculation, showing that the two-band Mott transition is heavily affected already at small $\Delta \ll W$, and not at $\Delta \sim W$, as one might have expected. As the DMFT calculations below show, the effective emptying transition occurs when Δ increases to reach $\Delta_c(U) \propto zW \propto (U_c^{2\text{-band}} - U)$.

Further quantitative informations concerning this phase diagram (in particular in the region of intermediate $U \sim W$ and $\Delta < W$) were obtained [140] by means of DMFT in the exact diagonalization flavor [155, 159] on the Bethe lattice. The results of the DMFT calculations are summarized in Fig. 6.11. The DMFT critical $U_c^{1\text{-band}} \simeq 1.35W$ and $U_c^{2\text{-band}} \simeq 1.8W$ are in fair agreement with corresponding values obtained by other methods [152, 158, 159, 189]. The other points in the phase diagram are obtained by following the stability of the two-band metal for a given value of U and increasing Δ , marking the emptying transition to the one-band metal or to the insulator.

A deficiency of this single-site DMFT calculation – which is restricted as usual to paramagnetic states only – is the absence of a two-band insulating state for $\Delta > 0$ (i.e. the M' point coincides with A). In fact, the suppression of the antiferro orbital

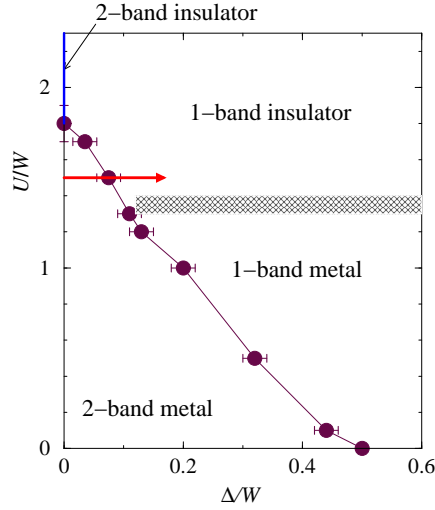


Fig. 6.11. DMFT zero-temperature phase diagram for the two-band Hubbard model at quarter filling (one electron per site), obtained by the exact diagonalization method in the paramagnetic sector. (From Ref. [140].)

fluctuations embodied in the exchange model (6.20) produces a fictitious infinite uniform orbital susceptibility which leads to full orbital polarization as soon as Δ is turned on [155]. Despite this limitation, the results of the DMFT calculations are suggestive, revealing the announced sharp reduction of the metal-insulator $U_c(\Delta)$ for small but finite Δ . Indeed, the DMFT yields a $\Delta_c(U)$ which is roughly proportional to the quasiparticle residue $z(U)$ of the undistorted ($\Delta = 0$) correlated metal at $U < U_c^{2\text{-band}}$,

$$\frac{\Delta_c(U)}{W} \propto \beta z(U), \quad (6.21)$$

with a proportionality constant $\beta \simeq 0.3$. Since $z(U)$ vanishes as $U \rightarrow U_c^{2\text{-band}}$, most likely linearly in $(U_c^{2\text{-band}} - U)$ [155], even a small $\Delta \ll W$ is sufficient to cause a metal-insulator transition in the strongly correlated metal. For example, following the bold arrow at $U = 1.5W$ in Fig. 6.11, a Δ value as small as $0.08W$ is sufficient to cross the transition line from the metal to insulator.

Illustrating further the transition, Fig. 6.12 shows the behavior of the spectral density

$$A_m(\omega) = -\pi^{-1} \text{Im} G_m(\omega),$$

$G_m(\omega)$ being the one-particle Green's function of band m , on both sides of the metal-insulator transition. The asymmetry of the upper-band spectral density $A_2(\omega)$ (solid lines) is very pronounced, as this band is nearly ($\Delta/W = 0.07$) or completely ($\Delta/W = 0.08$) empty. As soon as the Kondo-like peaks of the two bands differ enough in energy to induce the emptying of band 2, the lower-band spectral density $A_1(\omega)$ takes the symmetric shape, characteristic of the half-filled one-band Hubbard model. Here the quasiparticle peak disappears completely, as this value of $U > U_c^{1\text{-band}}$ puts the Hubbard model of band 1 well inside the insulating regime.

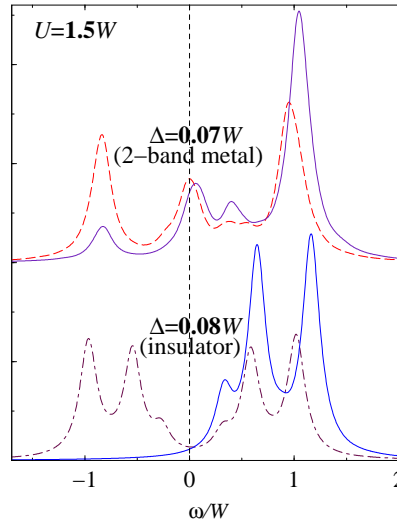


Fig. 6.12. Spectral density $A_m(\omega) = -\pi^{-1}\text{Im}G_m(\omega)$ at $U/W = 1.5$ across the Mott-Hubbard transition for increasing anisotropy splitting Δ . ω is referred to the Fermi energy. Solid lines refer to the minority orbital $m = 2$. The multi-peak structures of the high-energy side bands are artifacts of the finite discretization of the conduction band. (From Ref. [140].)

6.4.2 Noncubic band splitting and correlations in $\text{NH}_3\text{K}_3\text{C}_{60}$

The above $d = 2$ model calculations show that a small splitting $\Delta \propto zW$ of the orbitally degenerate band can drive the metal-insulator transition. We wish to explore the implications that this result – if assumed to be more general than the simple model where it was derived – can have on the metal-insulator transition which takes place between isoelectronic K_3C_{60} and $\text{NH}_3\text{K}_3\text{C}_{60}$ (the former cubic and the latter orthorhombic) and on the insulator-metal transition of $\text{NH}_3\text{K}_3\text{C}_{60}$ itself under pressure.

The effect of ammoniation is apparently twofold. The first effect is a large volume expansion, implying some band narrowing as well as an increase of U due to reduced screening. The second effect is a breaking of cubic symmetry in the anisotropic lattice structure. The actual strength of anisotropy in the ammoniated fulleride may be estimated quantitatively from the DFT-LDA bands of Fig. 6.6. They were obtained in a simplified geometry with a single C_{60} unit cell with lattice constant $a = 14.2 \text{ \AA}$ for fcc K_3C_{60} , and $a = 14.89 \text{ \AA}$ for $\text{NH}_3\text{K}_3\text{C}_{60}$ the latter with a centered tetragonal unit cell with $c/a = 0.91$, neglecting the exceedingly small difference between a and b . Merohedral disorder and the rich antiferro-rotational structure recently discovered in actual $\text{NH}_3\text{K}_3\text{C}_{60}$ [194] are also ignored. The bands indicate that the insertion of the NH_3 molecules modifies only weakly the essentially pure K_3C_{60} LUMO conduction band, as expected. In particular, as apparent from Fig. 6.6, the DFT-LDA bandwidths of $\text{NH}_3\text{K}_3\text{C}_{60}$ and K_3C_{60} are very similar, both $W \sim 0.6 \text{ eV}$. The main difference in the two band structures is a splitting of the threefold-degenerate t_{1u} band of K_3C_{60} at the Γ point of $\text{NH}_3\text{K}_3\text{C}_{60}$. The Γ -point splitting,

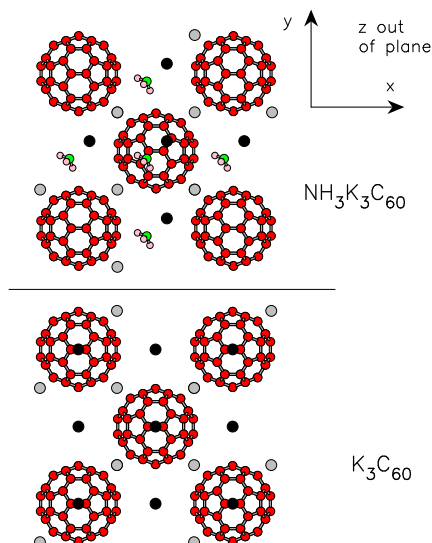


Fig. 6.13. Simplified geometry of $\text{NH}_3\text{K}_3\text{C}_{60}$ (top) and K_3C_{60} (bottom) used in the DFT-LDA calculation. Octahedral K atoms are indicated in black, while tetrahedral ones are in gray. All visible atoms of the central unit cell are shown together with some atoms in the neighbor unit cells. In $\text{NH}_3\text{K}_3\text{C}_{60}$ the c -axis is in the z direction. (From Ref. [140].)

roughly corresponding to a dimensionless ratio $\Delta/W \sim 0.25$, provides a measure of the strength of the non-cubic crystalline environment seen by the t_{1u} orbital on each fullerene molecule in the orthorhombic structure of $\text{NH}_3\text{K}_3\text{C}_{60}$. Its magnitude is roughly a quarter ($0.2 - 0.3$) of the total bandwidth; this represents the main result of this DFT calculation. Now if this compound were an uncorrelated metal, this splitting would have no real consequences, besides a change of shape of the Fermi surface. The consequences can be much more important due to strong correlations, as anticipated above.

In fact, as discussed above, the fullerides lie on the metallic side of the Mott transition in the half-filled $d = 3$ band cubic system. Upon ammoniation of K_3C_{60} into orthorhombic $\text{NH}_3\text{K}_3\text{C}_{60}$, the volume expansion will first of all increase U/W , while the anisotropy will give rise to a nonzero Δ , corresponding to a displacement as indicated by a rightward arrow in Fig. 6.11. Inspection of Fig. 6.11 shows that, if U is close enough to U_c , even a band splitting Δ substantially smaller than what we have estimated for $\text{NH}_3\text{K}_3\text{C}_{60}$ could suffice to drive that metal insulator transition, even without any appreciable change in U/W . Conductivity measurements [195] on the class of compounds $\text{NH}_3\text{K}_{3-x}\text{Rb}_x\text{C}_{60}$ supports the possibility that the orthorhombic distortion could be an important ingredient driving the Mott transition in these systems. An interesting – even if perhaps not practically straightforward – test of this overall picture could be obtained by applying uniaxial stress to cubic superconducting fullerides of the A_3C_{60} family. Contrary to the standard tendency

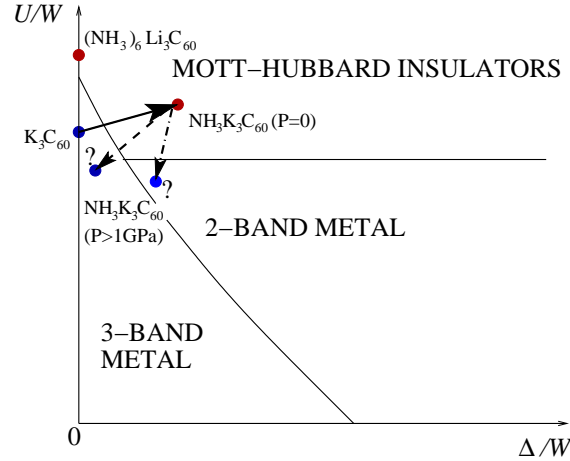


Fig. 6.14. A schematic (U, Δ) phase diagram for the $d = 3$ -bands family of compounds K_3C_{60} and $NH_3K_3C_{60}$. The dashed and dot-dashed arrows indicate two plausible paths of pressure-induced metallization of $NH_3K_3C_{60}$. Cubic insulating $(NH_3)_6Li_3C_{60}$ [12] is also indicated. (Adapted from Ref. [140].)

of hydrostatic pressure toward metallization and lower superconducting T_c , the orbital splitting associated with the appropriate uniaxial strain could drive some of these compounds towards stronger correlation, thus possibly first toward higher T_c , and eventually Mott insulating. A similar suggestion was put forward by Koch [196], although on rather different grounds.

We must stress here that the scenario sketched above does not at all diminish the role, in the metal-insulator transition, of the accompanying expansion of the lattice, and of the dependence of U/W upon volume. That role is experimentally proven by the observation of a pressure-driven insulator-metal transition, where $NH_3 K_3C_{60}$ is transformed into a metal (and a superconductor), despite the permanence of the orthorhombic structure [170].

6.4.3 Mott transition in other fullerides and other molecular conductors

The vicinity to the metal-insulator transition is not exclusive of $NH_3 A_3C_{60}$. Other systems of the same family are $(NH_3)_6Li_3C_{60}$ [12], $(NH_3)_x NaRb_2C_{60}$ ($x \simeq 1.6$) [197], $(NH_3)_x NaK_2C_{60}$ ($0.5 < x < 1$) [198, 199, 200], and the noncubic expanded alkali fulleride Cs_3C_{60} [201]. The pressure-driven insulator-superconductor transition observed in the latter compound further underscores the role of volume expansion in favoring the Mott insulator. In fact, $(NH_3)_6Li_3C_{60}$ is an example of a compound of the $n = 3$ family lying beyond the Mott transition despite its cubic structure [12], as illustrated in Fig. 6.14.

The $n = 4$ alkali fullerides also sit in the vicinity of the metal-insulator transition, usually on the insulating side. Indeed, the pressure-induced insulator to metal transition observed in tetragonal Rb_4C_{60} [126] is reminiscent of that observed in the

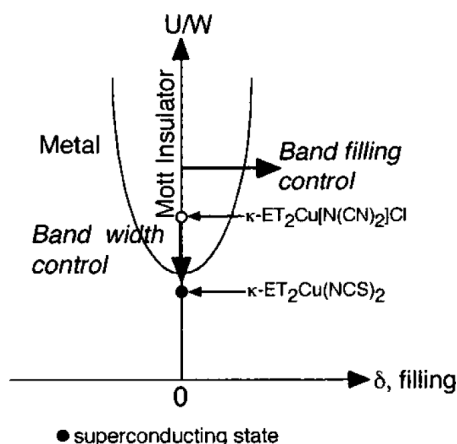


Fig. 6.15. Figure 1. Electronic phase diagram of organic conductors. The vertical axis indicates electron correlation U/W . The organic antiferromagnetic Mott insulating state (κ -ET₂Cu[N(CN)₂]Cl) transforms into a superconducting one [κ -ET₂Cu(NCS)₂], with a reduction in U/W . The horizontal axis shows the band-filling control. (From Ref. [202].)

C_{60}^{3-} compounds $NH_3 K_3 C_{60}$ and $Cs_3 C_{60}$, but for the lack of superconductivity. We shall come back to these C_{60}^{4-} compounds in the final discussion.

In the wider class of molecular conductors, the Mott transition is not exclusive of the fullerenes; other organic compounds show a similar phase diagram. Especially the κ -ET₂ [ET = bis(ethylenedithio)tetrathiafulvalene] compounds show a similar phenomenology to trivalent fullerenes [202], with a clear Mott transition at stoichiometry and a superconducting phase all around, Fig. 6.15. More recently, insulating metal-phthalocyanine organic films were turned conducting and metallic by alkali doping [203, 204]. A similar scheme to fullerenes, and to the metallic organics, has been proposed [205] as a possible scenario for the electron-doped metal-phthalocyanine conductors. The verification of the existence of stoichiometric phases, of Mott insulators at integer fillings, and possibly of superconducting phases in between remains a challenge for future experiments and theory in these materials.

Next, we should mention compounds such as $(AsF_6)_2 C_{60}$ [61, 62, 63, 64], where fullerene is stripped of two of its h_u valence electrons. The physics of positive C_{60} ions has been described in Ref. [105], and is somewhat parallel to that of negative ions, though with a richer parameter space which implies several complications. The Hubbard U in the h_u HOMO level is slightly larger than in t_{1u} LUMO. Cancellation between Hund's rule exchange and JT effect, discussed in sections 6.2.4 and 6.4.4, is present here too. It was calculated to be nearly exact in the doubly positive ion, with a slight prevalence of exchange and a marginally stable high-spin ground state [105]. The doubly doped-solid state compounds $(AsF_6)_2 C_{60}$ and $(SbF_6)_2 C_{60}$ have been reported to be small gap insulators [61, 62, 63, 64]. There appears to be no simple way that they could be band insulators, and the likeliest explanation is that they are Mott insulators. As for magnetism, some indirect experimental evidence has been suggested, consistent with high spin in the di-cation. However the balance between

intramolecular exchange and JT is very marginal, which leaves the possibility for a low-spin hole-doped Mott insulator wide open. There is even some preliminary indication that this might in fact be realized in $(\text{AsF}_6)_2\text{C}_{60}$ [206]. It would be very interesting in this respect to begin an experimental study of the insulator-metal transition in these compounds, to be obtained for example by hydrostatic pressure. Especially if the transition was relatively continuous and not too strongly first-order, the ensuing metallic phase close to the singlet Mott insulator should exhibit a pseudogap with strong pair correlations, and possibly superconductivity, similar to that described in Ref. [191].

Finally, we note that the pressure- or doping-induced transformation of Mott insulators into metals and strongly correlated superconductors which we discuss here for fullerene compounds, is a scenario which shares many important elements with the high- T_c cuprates. Again, this is an issue to which we will return later.

6.4.4 The crucial role of exchange and of JT on-site interactions

While the above bare Hubbard model defines the main backbone of the phase diagram, the precise details depends strongly on a variety of secondary, on-site couplings, generally present as permitted by the orbital degeneracy of the site. They act as a rule such as to optimize the energetics of the isolated site. As such, they generally favor the Mott insulating state, where electrons effectively localize on site. In the metallic state, conversely, kinetic energy washes out much more the effect of these on-site couplings. Electrons in the insulating state where on-site occupancy is close to integer and poorly fluctuating, can take full advantage of these secondary couplings, whereas travelling electrons in the metallic state cannot. As a result the overall effect of secondary on-site couplings such as J and E_{JT} is to reduce the critical U_c . On the contrary, we can expect that strongly nonlocal/intersite couplings could favor the metallic state, and raise U_c . In the fullerenes, intramolecular couplings dominate, while screening may be assumed to suppress the long-range interactions. In particular, while we certainly cannot rule out some role for an inter-molecular Coulomb interaction V , we will completely neglect it here.

As has been repeated over and over, the two important intra-site interactions are the JT coupling, Eq. (6.4), and the Hund's rule exchange part of Eq. (6.11). In the DMFT calculation of Sec. 6.4.1 however, these terms were initially left out. In fact, these on-site interactions, even if small in comparison with U and W , play a crucial role on the Mott transition in a band-degenerate conductor. Their presence can actually change nearly everything: the nature of the Mott insulator, its spin and orbital contents, the nature of the metal phase, its tendency to superconduct or not, and of course the precise location U_c of the Mott transition itself. Probably the simplest manner to illustrate this physical situation is to describe the results of DMFT calculations with proper inclusion of on-site interactions.

On a given molecular ion, Hund's rule exchange will favor maximum spin and maximum orbital momentum, while JT will favor just the opposite. Because, as explained in Sec. 6.2.4, there is an important cancellation between the two, neither of them can be safely neglected. Without entering here any of the technical details, it is difficult to solve the DMFT problem including exactly both these intra-site couplings, and some approximation must be made. Very detailed DMFT work has been done including a realistic representation of the electron-vibrational JT coupling for the fullerenes. In particular, Refs. [111, 207, 208] study a $d = 3$ Hubbard-Holstein

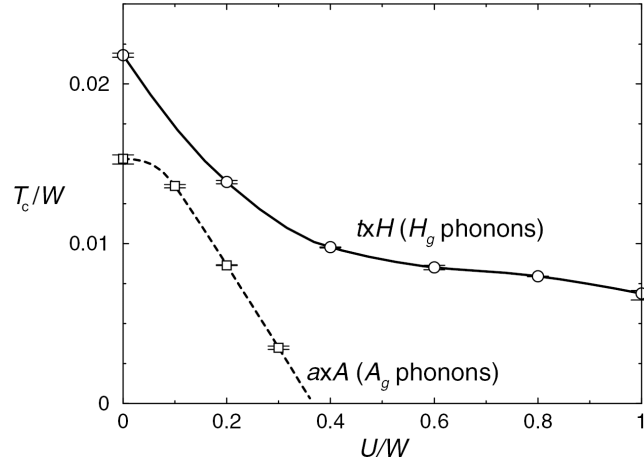


Fig. 6.16. Superconducting T_c as a function of U for the $t \otimes H$ and $a \otimes A$ models for the half filled $d = 3$ model, treated within the DMFT. The parameters are $\lambda = 0.6$ and $\omega/W = 0.25$. The figure illustrates the important difference between H_g and A_g phonons. (From Ref. [207].)

model including a single JT H_g phonon mode (5 oscillators rather than 40). The role of different lattice symmetry is investigated in Ref. [208]. These approaches employ very accurate and extensive quantum Monte Carlo calculations in a finite cluster, including the vibronic coupling with realistic JT strength λ and a realistic band structure. (An earlier calculation [185] even investigated the role of disorder in these systems). Reference [207] addresses mainly superconductivity in the $d = 3$ Hubbard-Holstein-JT model. As illustrated in Fig. 6.16, it was found (like in the $d = 2$ model) that the JT coupling to degenerate phonons produces a pairing much more compatible with strong correlations (large U) than coupling to a single non-JT A_g mode. In non-JT A_g electron-phonon coupling superconductivity disappears when $\mathcal{U}_n = U + U^{e-v} \geq 0$, while in JT H_g coupling superconductivity survives up to largely repulsive $\mathcal{U}_n > 0$. On the other hand, for small U , the local pairing becomes generally less efficient, because charge fluctuations induced by electron hopping disrupt the JT ground state(s) into uncorrelated electron pairs. Hence the superconducting order parameter is always depressed by U at small U . As U is increased, coherent electron hopping is gradually suppressed and the local pair formation becomes more important. For realistically large JT coupling $\lambda = \frac{5}{6} N(\epsilon_F) \sum_k g_k^2 \hbar \omega_k \sim 1$ [16, 93] $d = n = 3$ and increasing U the metal phase below U_c is always superconducting, with T_c a monotonically decreasing function of U . In other words, electron-electron repulsion always disfavors superconductivity for realistically large JT coupling [207].

However, this approximation is unrealistic as it neglects Hund's rule exchange, and the large cancellation of JT energetics that it implies. Inclusion of exchange is difficult, because it leads to a fermion sign problem in the Monte Carlo DMFT impurity solver. If on the other hand the impurity is solved by, e.g., Lanczos diagonalization, exchange can be treated but the phonon ladder gives rise to too many states per each site. An approximate way out is available very close to the Mott transition. Here the quasiparticle bandwidth zW tends continuously to zero, and sufficiently

close to U_c it falls below the typical vibrational frequency $\hbar\omega$. In this regime, the frequency dependence of the retarded JT coupling (assumed to be weak) can be integrated out, resulting simply in an additional but inverted Hund's rule like exchange term. As discussed in Sec. 6.2.4, for $d = 3$ that term is $J^{e-v} = -\frac{3}{4} \sum_k g_k^2 \hbar\omega_k$. In this limit – close enough to the Mott transition, JT coupling not too strong, relatively high vibration frequencies – it is therefore possible to treat both Hund's rule exchange and JT coupling, by simply replacing J with $J_{\text{eff}} = J + J^{e-v}$. This is the route generally followed in recent work by M. Capone *et al.* [146, 186, 190, 191] and by M. Granath and S. Östlund [209].

In the t_{1u} molecular level of fullerene $J \simeq 50$ meV, and the DFT-LDA JT couplings of Ref. [70] yield $J^{e-v} = -57$ meV, while the couplings obtained from photoemission [93] are consistent with $J^{e-v} = -127$ meV: with both estimates the net resulting J_{eff} is negative. The effective Hund's rule of C_{60}^{n-} is then inverted, the low-spin states representing the ground state, as dictated by JT coupling. It is important to underline again here that the massive cancellation finally leaves fullerenes with a *weak* on-site spin pairing interaction, replacing the original stronger couplings, both JT and Hund. The consequences of this weak residual pairing are, as it turns out, qualitatively different from either the strong singlet pairing required by JT alone, or by the strong triplet pairing required by Hund's J . Similarly, in the half filled e_g molecular level of a metal phthalocyanine ($d = n = 2$) it is predicted $J_{\text{eff}} = -60$ meV [205], again inverted, but again small as a result of a strong cancellation.

Let us consider in detail the consequences of this cancellation and of the final Hund's rule inversion. The first consequence is that the nature of the Mott insulator itself is affected. Since the isolated molecular ion ground state has low spin (a spin singlet for even n and a spin doublet for odd n), so will the Mott-insulator sites. The insulating state is more complicated and intriguing than either the one-band Mott insulator, or the simple orbitally-ordered cooperative JT distorted state. It is rather a Mott Jahn-Teller insulator. Let us try a description of that state, in the easy case of $n = 2$ electrons/site. Assume initially zero hopping between sites. On each site, the JT phonons are characterized by a 2-dimensional (pseudo)rotor in the trough. Subject to its own quantum fluctuations, this free rotor favors no special direction and will have its (say) $L = 0$ ground state separated by a gap δ from its $L = 1$ first excited state. Turning now on a hopping $\propto W$ between sites, this will cause an intersite interaction between rotors of order W^2/U . If that is strong enough, the rotors will freeze statically in an orbitally ordered state, similar to a ferroelectric, which is on fact a cooperative JT distortion [76, 102, 103, 210]. If instead the on-site quantum fluctuations make δ large enough, then the static cooperative order will quantum mechanically melt. This quantum melted state, the rotor analogue of a spin singlet, is the Mott-JT state [211]. This state bears some resemblance to the quantum paraelectric state [212]. It is strongly nonadiabatic in nature, which reflects in a strongly entangled admixture of electronic and phonon states: all electronic spectroscopies should observe radically renormalized and vibronically broadened “bands”, even at low temperature. Other molecular and lattice properties of this state still need to be worked out and investigated. This remains a theoretical task for the future.

Further characterization of the Mott-JT state is needed, both theoretically and experimentally, especially when it comes to its spectroscopical properties. The main examples at our disposal are $\text{NH}_3 \text{K}_3\text{C}_{60}$ (orthorhombic) [194] and $(\text{NH}_3)_6\text{Li}_3\text{C}_{60}$ (cubic) [12] for $n = 3$ and a $S = 1/2$ on-site ground state, and prominently Rb_4C_{60} ,

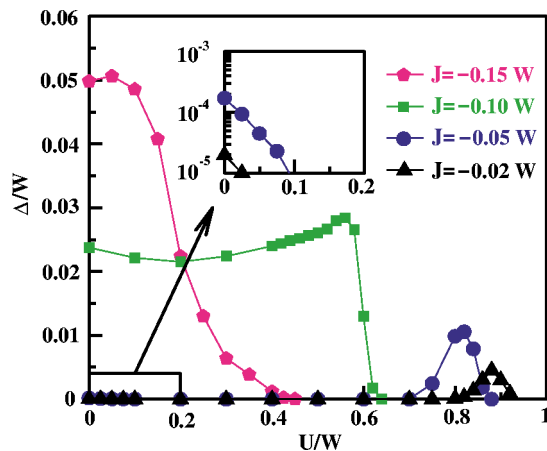


Fig. 6.17. Superconducting gap in a half-filled $d = 2$ -band model, as a function of the on-site repulsion for several (anti-Hund) couplings $J \equiv J_{\text{eff}} = J + J^{e-v}$ (where J^{e-v} accounts antiadiabatically for the electron-phonon interaction if $J^{e-v} = -\lambda/[2N(\epsilon_F)] = -2g^2\hbar\omega$, and $g\hbar\omega$ represents the coupling strength of the $e \otimes E$ JT coupling at each site; the difference with the relation of Table 6.2 is due to $d = 2$ rather than $d = 3$). Increasing repulsion spoils superconductivity at strong electron-phonon coupling. Superconductivity is instead strongly enhanced close to the Mott transition at weak coupling. The inset reports the weak-coupling regime on an expanded scale, showing a much smaller gap at small U compared to $U \simeq U_c$. (Adapted from Ref. [146].)

K_4C_{60} for $n = 4$, $S = 0$ singlet ground state. Concerning the $n = 3$ Mott insulators, the main evidence so far is their clear characterization as spin-1/2 antiferromagnets. Since there are 3 electrons/fullerene, that can be explained only by a JT- dominated state. That state could be at this stage either a statically distorted, collective JT insulator, or a quantum melted Mott-JT state. The available crystal and magnetic structure of orthorhombic $\text{NH}_3 \text{K}_3\text{C}_{60}$ [168, 194] displays a very rich interplay of magnetic and orbital order, which is only well analysed but is apparently compatible with either possibilities. It should be noted in addition that merohedral disorder in the relative angular orientation of the C_{60} molecules will frustrate static collective order, additionally favoring the melted state. Indeed only in the well ordered, “discrete” salts well defined collective distortions have been observed so far [15]. An orbitally-ordered static collective JT state [76, 102, 103, 210] has never been reported in the alkali fullerenes [213]. On the other hand, in a band-degenerate context, the possibility of dynamical orbital order should always be considered [211]. The question whether one or more of the existing Mott insulating fullerenes could be characterized as a dynamical Mott Jahn Teller insulator stands at this stage as an exciting experimental challenge.

After this illustration of the important effects of on site interactions on the mott insulating fullerenes, we can now move on to the metallic phase, obtained at smaller U values. As we will see, the metallic phase below U_c is even more affected, and in fact it often becomes superconducting. This is not in itself totally surprising, since we have

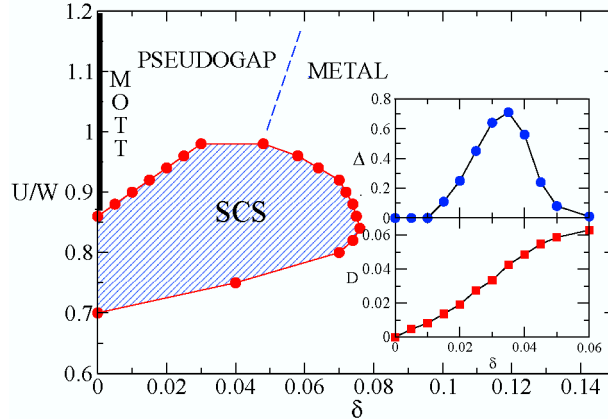


Fig. 6.18. Phase diagram of the $d = 2$ model as a function of U/W and doping $\delta = n - 2$ at $J_{\text{eff}} = -0.05W$. The thick vertical line marks the singlet Mott insulator. For $U = 0.92W$, the inset shows the superconducting gap divided by a factor 3 and the Drude weight D (i.e. the strength of the superfluid peak normalized to the noninteracting value) as functions of doping. (From Ref. [146].)

after all a small but definitely attractive J_{eff} reflecting a locally dominant electron-vibration coupling (even if orders of magnitude smaller than the repulsive U !). What is more surprising is the behavior of the superconducting gap as a function of U , see Fig. 6.17. So long as $(-J_{\text{eff}})$ is large – as in the uncompensated JT case described earlier – the gap decreases monotonically with increasing U . But when $(-J_{\text{eff}})$ is small – reflecting a strong cancellation by Hund’s rule – superconductivity only survives near $U = 0$ and near $U = U_c$. Superconductivity near the Mott transition was designated “strongly correlated superconductivity” (SCS). In SCS, the gap near U_c can increase for increasing U , and is many orders of magnitude larger than even the repulsion-free BCS-like superconducting gap near $U = 0$. Moreover, close to the Mott insulator, the SCS gap magnitude – and thus presumably the superconducting T_c – has a characteristic bell-shaped behavior.

The non-superconducting, metallic phase obtained by slightly doping the Mott-JT insulator at $U > U_c$ away from stoichiometry is also strongly unconventional, in that it has a pseudogap. Even if doping away from stoichiometry is not straightforward in fullerenes, this aspect of the theoretical phase diagram is quite illuminating. The presence of the pseudogap is related to $J_{\text{eff}} < 0$ and thus to the slightly prevailing JT effect, but is not at all bipolaronic, since as illustrated in Ref. [191] the electron occupancy of each site in this state is strongly pinned to the mean value n , the bipolaronic disproportionation into $(n - 1)$ and $(n + 1)$ pairs completely suppressed and in fact reversed by the large Hubbard U . Upon further doping of the pseudogap metal, the model exhibits SCS, the maximum gap attained at some optimal doping, then dropping and disappearing in a final overdoped phase. as shown in the overall $T = 0$ phase diagram of the $d = 2$ $n \simeq 2$ model reported in Fig. 6.18.

As one can see, many of these features are very reminiscent of high- T_c cuprates, whereas the model does not describe cuprates at all. Here we have on-site orbital degeneracy, Hund’s rule exchange, and JT coupling, all elements that are absent or

otherwise quite different in the cuprates. The strongly correlated superconducting order parameter in the model is, as in actual fullerides, s-wave and not d-wave as in the cuprates. We suggest that our models and at least some of the fullerides which they describe, are new members of a wider family of strongly correlated superconductors, which includes the cuprates, and all potentially high- T_c materials.

In this light, it is important to extract and to expose our overall qualitative understanding out of the model calculations. The occurrence of superconductivity in our orbitally degenerate molecular conductors, meant to model the fullerides, can be qualitatively rationalized by discussing what happens at integer filling as U is raised to approach the Mott insulating transition at U_c . First, the quasiparticle bandwidth narrows indefinitely, from W to zW with $z \rightarrow 0$ as $U \rightarrow U_c$. The rest of the single-particle spectral weight moves to the incoherent Hubbard bands, far away from the Fermi level. Second, since all charge fluctuations are gradually frozen out when approaching the Mott insulator, so are all the charge-related repulsions (and for that matter, attractions too) between the quasiparticles. For example, U is effectively reduced to $\sim zU$, and very near the Mott transition the propagating quasiparticles tend to infinitely massive interacting fermions, with a decreasing absolute repulsion. Third, thanks to the orbital degeneracy the spin fluctuations are not frozen out, and so attractions that act in the spin channel are not renormalized away. Therefore, e.g. the effective Hund-rule exchange J or J_{eff} retains its bare value even at the Mott transition, and that can easily overcome the weak repulsion zU .

These three elements make the effective quasiparticle Hamiltonian very similar to an *attractive* Hubbard model, with a bandwidth zW and an on-site attraction $J_{\text{eff}} < 0$. The ground state is a weak-coupling BCS-like superconductor, at least sufficiently below the Mott transition, so long as $zW \gg |J_{\text{eff}}|$. As U grows, the superconductivity changes from weak to strong coupling, the maximum gap achieved when $zW \sim |J_{\text{eff}}|$. This point is equivalent to the maximum of the Nozières-Schmitt-Rink [214, 215] curve of T_c versus λ in purely electron-phonon superconductors and, we believe, also to the optimal doping point in the cuprates.

If assumed to hold quantitatively, the qualitative mapping onto the attractive Hubbard model has the additional virtue of even predicting the maximum 3D critical temperature of our type of model at optimal doping, by reading it off the attractive Hubbard model studies. That gives approximately $k_B T_c^{\text{max}} \sim 0.07 |J_{\text{eff}}|$ for our models. In trivalent fullerides the value of $|J_{\text{eff}}|$ can be extracted by equating the observed spin gap ~ 140 meV [127, 128] to $5 |J_{\text{eff}}|$ (see Table 6.4), yielding $T_c^{\text{max}} \simeq 0.07 |J_{\text{eff}}|/k_B \simeq 23$ K, which is surprisingly, though probably unfairly, accurate.

One remaining question is: what is the relationship of this “island” of SCS near the Mott transition, to the more standard BCS-like phonon driven superconductivity one finds in the same model when there is no electron-electron repulsion, i.e. near $U = 0$? The answer to this question is very instructive, and is obtained by solving the model for a grid of on-site attractive coupling values – negative J_{eff} values [146]. As shown by the plot of zero temperature superconducting gaps in Fig. 6.17 if $|J_{\text{eff}}|$ is large, then the pairing gap is in fact maximum at $U = 0$, and decreases monotonically for increasing U , vanishing just at the Mott transition. This scenario is, we believe, equivalent to that presented by Han *et al.* for $d = n = 2$ [216] and $d = n = 3$ [111, 207, 208]. In particular, the monotonic decrease of T_c as U approaches U_c in Fig. 6.19 (squares) is equivalent to the large- $|J_{\text{eff}}|$ monotonic gap of Fig. 6.17 in a

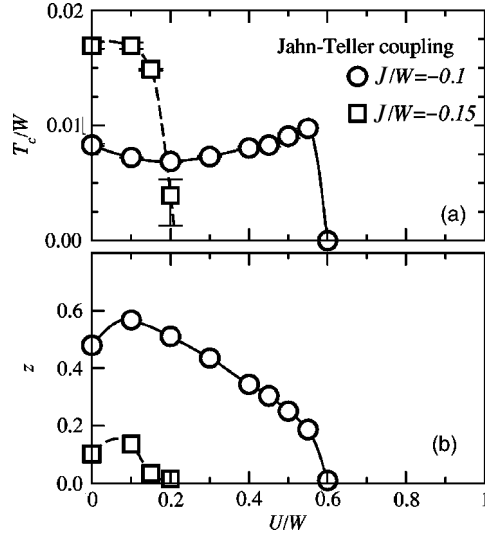


Fig. 6.19. (a) Superconducting transition temperature T_c vs Coulomb repulsion U in a $d = 2$ -band model with JT electron-phonon coupling, where the coupling strength $g\hbar\omega$ is gauged by $J = J^{e-v} = -2g^2\hbar\omega$. Weak JT phonon coupling ($J/W = -0.1$) produces superconductivity with a crossover from the conventional superconductivity (small U) to the local pairing regime at large U (a Mott-JT insulator). (b) Quasiparticle renormalization factor z . (Adapted from Ref. [216].)

model including explicitly the JT phonons. Similarly, the surge in T_c in Fig. 6.19 (circles) is essentially identical to that found earlier for small attractive $|J_{\text{eff}}|$.

Things do change qualitatively when the effective attraction decreases, as the dominance of JT is more and more eroded and cancelled by Hund's rule exchange. For decreasing $|J_{\text{eff}}|$, superconductivity remains strongest at $U = 0$ and near the Mott transition, but it gradually weakens in between. Eventually for very small $|J_{\text{eff}}|$ one arrives at two separate superconducting islands, one with a tiny BCS gap near $U = 0$, and a second one, near the Mott transition at U_c , with a gap orders of magnitude larger than BCS. This the SCS island. At the lower edge of this island (equivalent to the “overdoped” regime of the cuprates), the pairing is again BCS like: but the gap and presumably T_c rises as the electron-electron repulsion increases, rather than the opposite. We believe that this regime could describe most of the trivalent fullerenes, and their gigantic T_c and susceptibility increase with volume expansion. In fact the whole curve of T_c versus increasing volume as presented, e.g., by Durand *et al.* [12] (Fig. 6.20) could in our view be roughly identified with the theoretical bell-shaped curve of gap versus increasing U of Fig. 6.17.

A corollary is that the highest T_c fullerenes should be extremely strong-coupling materials, comparable to cuprates. This is in agreement with the extremely large H_{c2} values observed experimentally as well as with the existence of an irreversibility line in the $H - T$ phase diagram [217]. Both features are presently unexplained and both are similar to cuprates.

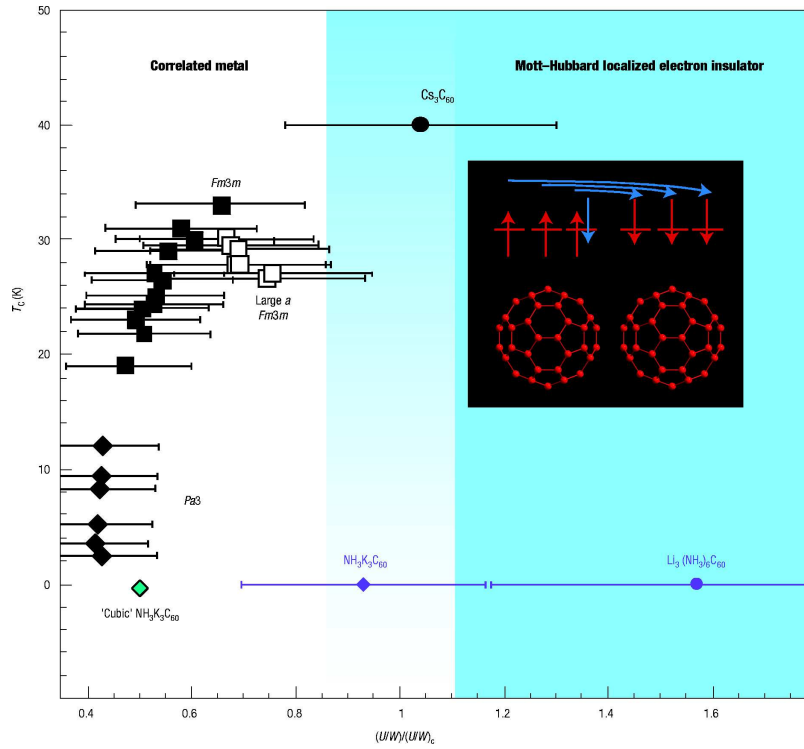


Fig. 6.20. A schematic phase diagram of C_{60}^{3-} fullerides. The superconducting transition temperature T_c is shown as a function of the ratio U/W divided by the critical value U_c/W required to produce electron localization – U_c/W is estimated to be 2.3 for the f.c.c. phases (square and diamond symbols), 1.3 for b.c.c. Cs_3C_{60} and $Li_3(NH_3)_6C_{60}$ (circles) and 1.1 for the orthorhombic $NH_3K_3C_{60}$. The value of U used to calculate U/W was 0.8 eV. The Mott-insulator region is shaded: uncertainties in the precise numerical estimates are emphasised by the graded shading of the crossover between metallic/superconducting and localized. W is derived for the f.c.c. phases from Ref. [2], for the orthorhombic $NH_3K_3C_{60}$ from Ref. [140] and for b.c.c. phases by DFT calculation [12]. The dramatic effect of lifted orbital degeneracy on the location of orthorhombic $NH_3K_3C_{60}$ is illustrated by comparison with an hypothetical “cubic” $NH_3K_3C_{60}$ retaining the t_{1u} orbital degeneracy and located well within the metallic regime. (From Ref. [12].)

The compounds in the descending T_c branch Fig. 6.20, apparently very close to the Mott transition, are the fulleride analog of the “underdoped” cuprates. They should be especially interesting, and their normal state should for example exhibit strong pseudogap features.

So far the discussion assumed prevalence of JT over Hund’s rule exchange, $J_{\text{eff}} < 0$. Also a hypothetical case of *positive* J_{eff} (regular Hund’s rule) would not be without interest. On-site high-spin states would prevail in this case. Again, as compared to $J = 0$, the Mott transition shifts to lower U_c [216]. This occurs for two reasons: a

reduction of the relevant pair energy \mathcal{U}_n proportional to J , and the fact that splitting of different Hund's multiplets opposes the metallic state. In the DMFT calculation of Ref. [216], the possibility of triplet superconductivity was investigated, and indeed it was found that before the metallic state turns into a magnetic Mott insulator, a superconducting phase emerges, with triplet pairing, but without p wave, thanks to the orbital degeneracy. If for example C_{60}^{2+} was really high spin in $(\text{AsF}_6)_2\text{C}_{60}$ or $(\text{SbF}_6)_2\text{C}_{60}$, among the metallic phases obtainable under pressure one could find one such triplet SCS.

In practice a small *negative* anti-Hund J_{eff} represents better the net balance of the positive Coulomb term and a prevailing electron-phonon attraction (assumed in the antiadiabatic limit) in C_{60}^{n-} [105, 106, 112]. Figure 6.17 shows that a strong reduction of U_c occurs under the action of an even small negative J_{eff} (as expected for any local interaction). In addition, as discussed in Sec. 6.2.4, a negative J_{eff} favors local low-spin states, which are spin singlets whenever the local occupancy is even. Of course, in the solid, band effects tend to favor local charge fluctuations and spin admixture, but as U approaches U_c , the bandwidth reduces effectively to the width zW of the Kondo peak. When zW becomes comparable to $|J|$, the local exchange term promotes locally paired singlets in a sort of anti-Migdal regime [176, 177, 178, 179, 180, 181] close to the transition, where the average phonon frequencies exceed the effective bandwidth. This regime favors superconductivity, and DMFT suggests that a high- T_c ($k_B T_c$ of order $|J_{\text{eff}}|$) superconducting phase should intrude between the metal and the low-spin Mott insulator [146, 186, 190, 191]. As shown in Fig. 6.17, for very small $|J_{\text{eff}}| \ll W$ (representative of the cancellation characteristic of C_{60}^{n-}), the very weak superconductivity of the uncorrelated regime $U \simeq 0$ becomes dominating close to the Mott transition. An alternative possibility to the intruding superconducting phase is a discontinuous, first-order transition, jumping directly from the metal to the insulator, and in fact this is a serious eventuality for the A_4C_{60} fullerenes, where no superconductivity is observed. The pressure-induced reversion from insulator to metal observed in tetragonal Rb_4C_{60} [126] is most likely the $n = 4$ counterpart of the $n = 3$ transition of the ammoniated compounds.

6.5 Conclusions

We have discussed some results and qualitative theoretical ideas on the modeling of metal-insulator transition in fullerene compounds. They have been described as Hubbard models with electron hopping with a bandwidth W between orbitally degenerate fullerene sites, each of them supporting a Coulomb repulsion U , a Hund's rule exchange J , and a JT distortion with energy gain E^{e-v} . The interplay of these parameters gives rise to a rich phase diagram, comprising Mott insulators, metals, and superconductors. For electrons in fullerene, the JT strength marginally prevails over exchange, a fact which has important implications for all phases. The Mott insulators can in reality become Mott-JT insulators, whose local configuration is low spin, with an electron-vibrational entanglement as intrinsic as that of a superconductor, and possibly displaying other unexplored features. The metal phases obtained by doping the even- n Mott insulators can possess a pseudogap, namely a depression of the density of states at the Fermi level, and a very reduced susceptibility, constituting a kind of nonadiabatic semimetals. The superconductor phases near the Mott insulators arise through pairing of quasiparticles, these constituting

a thin conducting web floating in a Mott-insulating sea. These model superconducting phases, although ultimately caused by JT effect (electron-phonon) and s-wave in character, are shown to share many features with those of high- T_c cuprates. This possibility calls for further experimental and theoretical work.

Further work should also be devoted to investigate the detailed nature of the Mott phase transition. The alternative possibilities of first-order and second-order transition, should be distinguished in the $n = 3$ and $n = 4$ classes of fullerides. For $n = 3$ compounds, the simultaneous disappearance of superconducting order and appearance of magnetic order seem theoretically incompatible with a continuous transition.

To investigate possible spin/orbital antiferro correlations of the kind observed in $\text{NH}_3 \text{K}_3\text{C}_{60}$ [194], one should study a detailed three-dimensional model, including the highly directional hopping matrix elements between different C_{60} sites (and possibly merohedral disorder). Some of these aspects could be addressed by standard mean-field techniques (of the type applied in a different context [218]), or quantum Monte Carlo cluster calculations which unfortunately suffer by significant finite-size effects. The DMFT method, based on an infinite lattice is free from these limitations, but the same aspects are inaccessible to a single-impurity DMFT model: cluster DMFT methods [183, 184] could lead to some progress in this direction.

Acknowledgments

We are indebted to V. Brouet, A. Goldoni, O. Gunnarsson, M. Fabrizio, R. Macovez, P. Rudolf and G. Santoro for useful discussions. This work was funded in part by the EU's Sixth Framework Programme through the Nanoquanta Network of Excellence (NMP4-CT-2004-500198). This work was partly supported by MIUR COFIN2003, MIUR COFIN2004, by FIRB RBAU017S8R operated by INFN, by MIUR FIRB RBAU017S8 R004, and by CNR-INFN (Iniziativa trasversale calcolo parallelo).

References

1. S. C. Erwin *Buckminsterfullerenes*, edited by W. E. Billups and M. A. Ciufolini (VCH Publishers, New York, 1993), p. 217.
2. S. Satpathy, V. P. Antropov, O. K. Andersen, O. Jepsen, O. Gunnarsson, and A. I. Liechtenstein, *Phys. Rev. B* **46**, 1773 (1992).
3. S. C. Erwin and C. Bruder, *Physica B* **199-200**, 600 (1994).
4. P. J. Benning, F. Stepniak, and J. H. Weaver, *Phys. Rev. B* **48**, 9086 (1993).
5. M. C. Martin, D. Koller, and L. Mihaly, *Phys. Rev. B* **47**, 14607 (1993).
6. M. J. Rosseinsky, D. W. Murphy, R. M. Fleming, and O. Zhou, *Nature (London)* **364**, 425 (1993).
7. Y. Iwasa and T. Kaneyasu, *Phys. Rev. B* **51**, 3678 (1995).
8. T. Takenobu, T. Muro, Y. Iwasa, and T. Mitani, *Phys. Rev. Lett.* **85**, 381 (2000).
9. T. T. Obu, H. Shimoda, Y. Iwasa, T. Mitani, M. Kosaka, K. U. Tanigaki, C. M. Brown, and K. Prassides, *Mol. Cryst. Liq. Cryst. Sci. Technol., Sect. A* **340**, 599 (2000).

10. H. Tou, Y. Maniwa, Y. Iwasa, H. Shimoda, and T. Mitani, *Phys. Rev. B* **62**, R775 (2000).
11. R. M. Fleming, M. J. Rosseinsky, A. P. Ramirez, D. W. Murphy, J. C. Tully, R. C. Haddon, T. Siegrist, R. Tycko, S. H. Glarum, P. Marsh, G. Dabbagh, S. M. Zahurak, A. V. Makhija, and C. Hampton, *Nature (London)* **352**, 701 (1992).
12. P. Durand, G. R. Darling, Y. Dubitsky, A. Zaopo, and M. J. Rosseinsky, *Nature Materials* **2**, 605 (2003).
13. A. P. Ramirez, *Supercond. Rev.* **1**, 1 (1994).
14. M. P. Gelfand, *Supercond. Rev.* **1**, 103 (1994).
15. C. A. Reed and R. D. Bolskar, *Chem. Rev.* **100**, 1075 (2000).
16. O. Gunnarsson, *Alkali-Doped Fullerenes: Narrow-Band Solids with Unusual Properties* (World Scientific, Singapore, 2004).
17. E. Schönherr, K. Matsumoto, and M. Wojnowski, *J. Crystal Growth* **146**, 227 (1995).
18. W. I. F. David, R. M. Ibberson, J. C. Matthewman, K. Prassides, T. J. S. Dennis, J. P. Hare, H. W. Kroto, R. Taylor, and D. R. M. Walton, *Nature (London)* **353**, 147 (1991); W. I. F. David, R. M. Ibberson, T. J. S. Dennis, J. P. Hare, and K. Prassides, *Europhys. Lett.* **18**, 219 (1992).
19. R. C. Haddon, L. E. Brus, and K. Raghavachari, *Chem. Phys. Lett.* **125**, 459 (1986); R. C. Haddon, T. Siegrist, R. Tycko, S. H. Glarum, P. Marsh, G. Dabbagh, S. M. Zahurak, A. V. Makhija, and C. Hampton, *Nature (London)* **352**, 701 (1992).
20. S. Satpathy, *Chem. Phys. Lett.* **130**, 545 (1986).
21. E. Bright Wilson, J. C. Decius, and P. C. Cross, *Molecular Vibrations, The Theory of Infrared and Raman Vibrational Spectra* (McGraw-Hill, New York, 1955).
22. A. Auerbach, N. Manini, and E. Tosatti, *Phys. Rev. B* **49**, 12998 (1994).
23. N. Manini, E. Tosatti, and A. Auerbach, *Phys. Rev. B* **49**, 13008 (1994).
24. A. Auerbach, *Phys. Rev. Lett.* **70**, 1874 (1994).
25. P. De Los Rios, N. Manini, and E. Tosatti, *Phys. Rev. B* **54**, 7157 (1996).
26. P. De Los Rios and N. Manini, *Recent Advances in the Chemistry and Physics of Fullerenes and Related Materials: Vol. 5*, edited by K. M. Kadish and R. S. Ruoff (The Electrochemical Society, Pennington, NJ, 1997), p. 468.
27. N. Manini and P. De Los Rios, *Proceedings of the XIV International Symposium on Electron-Phonon Dynamics and Jahn-Teller Effect*, ed. by G. Bevilacqua, L. Martinelli and N. Terzi (World Scientific, Singapore, 1999), p. 37.
28. N. Manini and P. De Los Rios, *J. Phys.: Condens. Matter* **10**, 8485 (1998).
29. N. Manini and P. De Los Rios, *Phys. Rev. B* **62**, 29 (2000).
30. C. P. Moate, M. C. M. O'Brien, J. L. Dunn, C. A. Bates, Y. M. Liu, and V. Z. Polinger, *Phys. Rev. Lett.* **77**, 4362 (1996).
31. C. P. Moate, J. L. Dunn, C. A. Bates, and Y. M. Liu, *J. Phys.: Condens. Matter* **9**, 6049 (1997).
32. N. Manini, *Phys. Rev. A* **71**, 032503 (2005).
33. D. S. Bethune, G. Meijer, W. C. Tang, H. J. Rosen, W. G. Golden, H. Seki, C. A. Brown, and M. S. de Vries, *Chem. Phys. Lett.* **179**, 181 (1991).
34. A. D. J. Haymet, *Chem. Phys. Lett.* **122**, 421 (1985).
35. F. Negri, G. Orlandi, and F. Zerbetto, *Chem. Phys. Lett.* **144**, 31 (1988).
36. W. H. Green Jr., S. M. Gorun, G. Fitzgerald, P. W. Fowler, A. Ceulemans, and B. C. Titeca, *J. Phys. Chem.* **100** 14892 (1996).

37. J. Kohanoff, W. Andreoni, and M. Parrinello, Phys. Rev. B **46**, 4371 (1992); J. Kohanoff, W. Andreoni, and M. Parrinello, Chem. Phys. Lett. **198**, 472 (1992); B. P. Feuston, W. Andreoni, M. Parrinello, and E. Clementi, Phys. Rev. B **44**, 4056 (1991).
38. M. R. Savina, L. L. Lohr, and A. H. Francis, Chem. Phys. Lett. **205**, 200 (1993).
39. S. Tomita, J. U. Andersen, E. Bonderup, P. Hvelplund, B. Liu, S. Brøndsted Nielsen, U. V. Pedersen, J. Rangama, K. Hansen, and O. Echt, Phys. Rev. Lett. **94**, 053002 (2005).
40. C. Yeretizian, K. Hansen, and R. L. Whetten, Science **260**, 652 (1993).
41. X. B. Wang, C. F. Ding, and L. S. Wang, J. Chem. Phys. **110**, 8217 (1999).
42. C. N. Yang, Rev. Mod. Phys. **34**, 694 (1962).
43. P. A. Limbach, L. Schweikhard, K. A. Cowen, M. T. McDermott, A. G. Marshall, and J. V. Coe, J. Am. Chem. Soc. **113**, 6795 (1991).
44. D. Dubois, K. M. Kadish, S. Flanagan, R. R. Haufler, L. P. F. Chibante, and L. J. Wilson, J. Am. Chem. Soc. **113**, 4364 (1991).
45. G. A. Heath, J. E. McGrady, and R. L. Martin, J. Chem. Soc., Chem. Commun. 1272 (1992).
46. W. K. Fullagar, I. R. Gentle, G. A. Heath, and J. W. White, J. Chem. Soc., Chem. Commun. 525 (1993).
47. M. Baumgarten, A. Gügel, L. Gherghel, Adv. Mater. **5**, 458 (1993).
48. E. Burstein, S. C. Erwin, M. Y. Jiang, and R. P. Messmer, Physica Scripta **T42**, 207 (1992).
49. S. Modesti, S. Cerasari, and P. Rudolf, Phys. Rev. Lett. **71**, 2469 (1993).
50. P. M. Allemand, K. C. Kemani, A. Koch, F. Wudl, K. Holczer, S. Donovan, G. Grüner, and J. D. Thompson, Science **253**, 301 (1991); K. Tanaka, A. A. Zakhidov, K. Yoshizawa, K. Okahara, T. Yamabe, K. Yakushi, K. Kikuchi, S. Suzuki, I. Ikemoto, and Y. Achiba, Phys. Lett. A **164**, 221 (1992).
51. V. N. Denisov, A. A. Zakhidov, G. Ruani, R. Zamboni, C. Taliani, K. Tanaka, K. Yoshizawa, T. Okahara, T. Yamabe, and Y. Achiba, Synth. Metals **55-57**, 3050 (1993).
52. A. F. Hebard, M. J. Rosseinsky, R. C. Haddon, D. W. Murphy, S. H. Glarum, T. T. M. Palstra, A. P. Ramirez, and A. R. Kortan, Nature (London) **350**, 600 (1991).
53. R. F. Kieff, T. L. Duty, J. W. Schneider, A. MacFarlane, K. Chow, J. W. Elzey, P. Mendels, G. D. Morris, J. H. Brewer, E. J. Ansaldo, C. Niedermayer, D. R. Noakes, C. E. Stronach, B. Hitti, and J. E. Fischer, Phys. Rev. Lett. **69**, 2005 (1992).
54. J. E. Fischer and P. A. Heiney, J. Phys. Chem. Solids **54**, 1725 (1993).
55. Y. Chabre, D. Djurado, M. Armand, W. R. Romanons, N. Coustel, J. P. McCauley Jr, J. E. Fischer, and A. B. Smith III, J. Am. Chem. Soc. **114**, 764 (1992).
56. J. Kohanoff, W. Andreoni, and M. Parrinello, Chem. Phys. Lett. **198**, 472 (1992); J. Kohanoff, PhD Thesis No. 10079 ETH Zurich (1993); W. Andreoni, *Electronic Properties of New Materials: Fullerenes*, Proceedings of the 1993 Kirchberg Winter School, edited by H. Kuzmany, J. Fink, M. Mehring, and S. Roth (Springer Verlag, Berlin, 1994).
57. S. Tomita, J. U. Andersen, C. Gottrup, P. Hvelplund, and U. V. Pedersen, Phys. Rev. Lett. **87**, 073401 (2001).

58. C. A. Reed, K.-C. Kim, R. D. Bolskar, and L. J. Mueller, *Science* **289**, 201 (2000).
59. C. Bruno, I. Doubitski, M. Marcaccio, F. Paolucci, D. Paolucci, and A. Zaopo, *J. Am. Chem. Soc.* **125**, 15738 (2003).
60. Z. Gasyna, L. Andrews, and P. N. Schatz, *J. Phys. Chem.* **96**, 1525 (1992).
61. W. R. Datars and P. K. Ummat, *Solid State Commun.* **94**, 649 (1995).
62. W. R. Datars, J. D. Palidwar, and P. K. Ummat, *J. Phys. Chem. Solids* **57**, 977 (1996).
63. A. M. Panich, P. K. Ummat, and W. R. Datars, *Solid State Commun.* **121**, 367 (2002).
64. A. M. Panich, H.-M. Vieth, P. K. Ummat, and W. R. Datars, *Physica B* **327**, 102 (2003).
65. A. Ceulemans, P. W. Fowler, and I. Vos, *J. Chem. Phys.* **100**, 5491 (1994).
66. K. Prassides, T. J. S. Dennis, J. P. Hare, J. Tomkinson, H. W. Kroto, R. Taylor, and D. R. M. Walton, *Chem. Phys. Lett.* **187**, 455 (1991); K. Prassides, C. Christides, M. J. Rosseinsky, J. Tomkinson, D. W. Murphy, and R. C. Haddon, *Europhys. Lett.* **19**, 629 (1992); R. A. Jishi and M. S. Dresselhaus, *Phys. Rev. B* **45**, 2597 (1992); M. G. Mitch, S. J. Chase, and J. S. Lannin, *Phys. Rev. B* **46**, 3696 (1992).
67. P. Zhou, K. A. Wang, Y. Wang, P. C. Eklund, M. S. Dresselhaus, G. Dresselhaus, and R. A. Jishi, *Phys. Rev. B* **46**, 2595 (1992).
68. G. Onida and G. Benedek, *Europhys. Lett.* **18**, 403 (1992).
69. Q. Jiang, H. Xia, Z. Zhang, and D. Tian, *Chem. Phys. Lett.* **192**, 93 (1992).
70. N. Manini, A. Dal Corso, M. Fabrizio, and E. Tosatti, *Philos. Mag. B* **81**, 793 (2001).
71. D. Balamurugan, M. K. Harbola, and R. Prasad, *Phys. Rev. A* **69**, 033201 (2004).
72. C. C. Chancey and M. C. M. O'Brien, *The Jahn-Teller Effect in C₆₀ and Other Icosahedral Complexes* (Princeton Univ. Press, Princeton, 1997).
73. P. H. Butler, *Point Group Symmetry Applications* (Plenum, New York, 1981).
74. M. C. M. O'Brien, *Phys. Rev.* **187**, 407 (1969).
75. M. C. M. O'Brien, *J. Phys. C* **4**, 2524 (1971).
76. I. B. Bersuker and V. Z. Polinger, *Vibronic Interactions in Molecules and Crystals* (Springer-Verlag, Berlin, 1989).
77. N. Koga and K. Morokuma, *Chem. Phys. Lett.* **196**, 191 (1992).
78. N. Manini, *Electron-Vibron Coupling in Charged Fullerene, Berry Phase, and Superconductivity*, PhD Thesis, (<http://www.sissa.it/cm/thesis/1995/manini.ps.gz> SISSA, Trieste, 1995).
79. K. Yabana and G. Bertsch, *Phys. Rev. B* **46**, 14263 (1992).
80. M. V. Berry, *Proc. R. Soc. London A* **392**, 45 (1984).
81. B. Goss Levi, *Phys. Today* **46**, 17 (1993).
82. J. Ihm, *Phys. Rev. B* **49**, 10726 (1994).
83. *Geometric Phases in Physics*, edited by A. Shapere and F. Wilczek (World Scientific, Singapore, 1989).
84. H. C. Longuet-Higgins, *Adv. Spect.* **2** 429, (1961), and references therein; G. Herzberg and H. C. Longuet-Higgins, *Discuss. Faraday Soc.* **35**, 77 (1963); H. C. Longuet-Higgins, *Proc. Roy. Soc. London A* **344**, 147 (1975); C. A. Mead and D. G. Truhlar, *J. Chem. Phys.* **70**, 2284 (1979).
85. C. A. Mead, *Rev. Mod. Phys.* **64**, 51 (1992).

86. J. P. Wolf, G. Delacrétaz, and L. Wöste, Phys. Rev. Lett. **63**, 1946 (1989); J. Blanc, M. Broyer, J. Chevalleyre, P. Dugourd, H. Kühling, P. Labastie, M. Ulbricht, J. P. Wolf, and L. Wöste, Z. Phys. D **19**,7 (1991); P. Dugourd, J. Chevalleyre, R. Antoine, M. Broyer, J. P. Wolf, and L. Wöste, Chem. Phys. Lett. **225**, 28 (1994).
87. G. D. Mahan, *Many-Particles Physics* (Plenum, New York, 1981).
88. M. Schlüter, M. Lannoo, M. Needels, G. A. Baraff, and D. Tománek, Phys. Rev. Lett. **68**, 526 (1991); J. Phys. Chem. Solids **53**, 1473 (1992).
89. C. M. Varma, J. Zaanen, and K. Raghavachari, Science **254**, 989 (1991).
90. V. P. Antropov, O. Gunnarsson, and A. I. Lichtenstein, Phys. Rev. B **48**, 7651 (1993).
91. J. C. R. Faulhaber, D. Y. K. Ko, and P. R. Briddon, Phys. Rev. B **48**, 661 (1993).
92. J. Winter and H. Kuzmany, Phys. Rev. B **53**, 655 (1996).
93. O. Gunnarsson, H. Handschuh, P. S. Bechthold, B. Kessler, G. Ganteför, and W. Eberhardt, Phys. Rev. Lett. **74**, 1875 (1995); O. Gunnarsson, Phys. Rev. B **51**, 3493 (1995).
94. N. Manini and E. Tosatti, Phys. Rev. Lett. **90**, 249601 (2003).
95. N. Manini, P. Gattari, and E. Tosatti, Phys. Rev. Lett. **91**, 196402 (2003).
96. P. Gattari, diploma thesis, University Milan (2003), <http://www.mi.infm.it/~manini/theses/gattari.pdf>.
97. P. Brühwiler, A. J. Maxwell, P. Balzer, S. Andersson, D. Arvanitis, L. Karlsson, and N. Mårtensson, Chem. Phys. Lett. **279**, 85 (1997).
98. S. E. Canton, A. J. Yench, E. Kukk, J. D. Bozek, M. C. A. Lopes, G. Snell, and N. Berrah, Phys. Rev. Lett. **89**, 045502 (2002).
99. A. Bordoni and N. Manini, *Fullerenes and Nanotubes - Materials for the New Chemical Frontier - Fullerenes - Vol. 14*, edited by P. V. Kamat, F. D'Souza, D. M. Guldi, and S. Fukuzumi (The Electrochemical Society, Pennington, NJ, 2005), p. 118.
100. L. Bergomi and T. Jolicoeur, Comptes Rendus Acad. Sci. II **318**, 283 (1994).
101. V. S. Langford and B. E. Williamson, J. Phys. Chem. A **103**, 6533 (1999).
102. G. A. Gehring and K. A. Gehring, Rep. Prog. Phys. **38**, 1 (1975).
103. M. D. Kaplan and B. G. Vekhter, *Cooperative Phenomena in Jahn-Teller crystals* (Plenum Press, New York, 1995).
104. N. Manini and E. Tosatti, *Recent Advances in the Chemistry and Physics of Fullerenes and Related Materials: Vol. 2*, edited by K. M. Kadish and R. S. Ruoff (The Electrochemical Society, Pennington, NJ, 1995), p. 1017.
105. M. Lüders, N. Manini, P. Gattari, and E. Tosatti, Eur. Phys. J. B **35**, 57 (2003).
106. M. Lueders and N. Manini, Adv. Quantum Chem. **44**, 289 (2003).
107. The incorrect values of g_k for the A_g modes published in Table 3 of Ref. [70] should be multiplied by a factor 2: in the present work we use the correct couplings.
108. A. Ceulemans, L. F. Chibotaru, and F. Cimpoesu Phys. Rev. Lett **78**, 3725 (1997).
109. G. Baskaran and E. Tosatti, Current Science (Bangalore) **61**, 33 (1991); S. Chakravarty, M. Gelfand, and S. Kivelson, Science **254**, 970 (1991); G. N. Murthy and A. Auerbach, Phys. Rev. B **46**, 331 (1992).
110. R. L. Martin and J. P. Ritchie, Phys. Rev. B **48**, 4845 (1993).

111. J. E. Han and O. Gunnarsson, *Physica B* **292**, 196 (2000).
112. M. Lüders, A. Bordoni, N. Manini, A. Dal Corso, M. Fabrizio, and E. Tosatti, *Philos. Mag. B* **82**, 1611 (2002).
113. A. V. Nikolaev and K. H. Michel, *J. Chem. Phys.* **117**, 4761 (2002).
114. A. H. H. Chang, W. C. Ermler, and R. M. Pitzer, *J. Phys. Chem.* **95**, 9288 (1991).
115. R. D. Cowan, *The Theory of Atomic Structure and Spectra* (Univ. of California Press, Berkeley-CA, 1981).
116. V. P. Antropov, O. Gunnarsson, and O. Jepsen, *Phys. Rev. B* **46**, 13647 (1992).
117. M. R. Pedersen and A. A. Quong, *Phys. Rev. B* **46**, 13584 (1992).
118. V. de Coulon, J. L. Martins, and F. Reuse, *Phys. Rev. B* **45**, 13671 (1992).
119. R. L. Hettich, R. N. Compton, and R. H. Ritchie, *Phys. Rev. Lett* **67**, 1242 (1991).
120. M. Wierzbowska, M. Lüders, and E. Tosatti, unpublished.
121. S. Chakravarty, S. Kivelson, M. I. Salkola and S. Tewari, *Science* **256**, 1306 (1992); S. R. White, S. Chakravarty, M. Gelfand, and S. Kivelson, *Phys. Rev. B* **45** 5062 (1992).
122. N. Berdenis and G. Murthy, *Phys. Rev. B* **52**, 3083 (1995).
123. F. Lin, J. Šmakov, E. S. Sørensen, C. Kallin, and A. J. Berlinsky, *Phys. Rev. B* **71**, 165436 (2005).
124. S. Sookhun, J. L. Dunn, and C. A. Bates, *Phys. Rev. B* **68**, 235403 (2003).
125. J. L. Dunn and H. Li, *Phys. Rev. B* **71**, 115411 (2005).
126. R. Kerkoud, P. Auban-Senzier, D. Jerome, S. Brazovskii, I. Luk'yanchuk, N. Kirova, F. Rachdi, and C. Goze, *J. Phys. Chem. Solids* **57**, 143 (1996).
127. G. Zimmer, M. Helme, M. Mehring, and F. Rachdi, *Europhys. Lett.* **27**, 543 (1994); G. Zimmer, M. Mehring, C. Goze, and F. Rachdi, *Phys. Rev. B* **52**, 13300 (1995); G. Zimmer, M. Mehring, C. Goze, and F. Rachdi, *Physics and Chemistry of Fullerenes and Derivatives*, edited by H. Kuzmany, J. Fink, M. Mehring, and S. Roth (World Scientific, Singapore, 1995), p. 452.
128. I. Lukyanchuk, N. Kirova, F. Rachdi, C. Goze, P. Molinie, and M. Mehring, *Phys. Rev. B* **51**, 3978 (1995).
129. P. Bhyrappa, P. Paul, J. Stinchcombe, P. D. W. Boyd, and C. A. Reed, *J. Am. Chem. Soc.* **115**, 11004 (1993).
130. C. Bossard, S. Rigaut, D. Astruc, M.-H. Delville, G. Felix, A. Fevrier-Bouvier, J. Amiell, S. Flandrois, and P. Delhaes, *J. Chem. Soc., Chem. Commun.* 333 (1993).
131. J. Chen, Z.-E. Huang, R.-F. Cai, Q.-F. Shao, and H.-J. Ye, *Solid State Commun.* **95**, 233 (1995).
132. P. D. W. Boyd, P. Bhyrappa, P. Paul, J. Stinchcombe, R. D. Bolskar, Y. Sun, and C. A. Reed, *J. Am. Chem. Soc.* **117**, 2907 (1995).
133. P. C. Trulove, R. T. Carlin, G. R. Eaton, and S. S. Eaton, *J. Am. Chem. Soc.* **117**, 6265 (1995).
134. Y. Sun, PhD Dissertation, University of Southern California (Los Angeles, CA, 1997).
135. V. Brouet, H. Alloul, F. Quere, G. Baumgartner, and L. Forro, *Phys. Rev. Lett.* **82**, 2131 (1999).
136. A. Schilder, H. Klos, I. Rystau, W. Schütz, and B. Gotschy, *Phys. Rev. Lett.* **73**, 1299 (1994).
137. D. P. Arovas and A. Auerbach, *Phys. Rev. B* **52**, 10114 (1995).

138. P. Paul, Z. Xie, R. Bau, P. D. W. Boyd, and C. A. Reed, *J. Am. Chem. Soc.* **116**, 4145 (1994).
139. S. C. Erwin and M. R. Pederson, *Phys. Rev. Lett.* **67**, 1610 (1991).
140. N. Manini, G. E. Santoro, A. Dal Corso, and E. Tosatti, *Phys. Rev. B* **66**, 115107 (2002).
141. O. Gunnarsson, S. C. Erwin, E. Koch, and R. M. Martin, *Phys. Rev. B* **57**, 2159 (1998).
142. E. L. Shirley and S. G. Louie, *Phys. Rev. Lett.* **71**, 133 (1993).
143. W. L. Wang, V. Brouet, X. J. Zhou, H. J. Choi, S. G. Louie, M. L. Cohen, S. A. Kellar, P. V. Bogdanov, A. Lanzara, A. Goldoni, F. Parmigiani, Z. Hussain, and Z.-X. Shen, *Science* **300**, 303 (2003).
144. A. Goldoni, contribution to present volume.
145. L. De Leo and M. Fabrizio, *Phys. Rev. Lett.* **94**, 236401 (2005).
146. M. Capone, M. Fabrizio, C. Castellani, and E. Tosatti, *Phys. Rev. Lett.* **86**, 5361 (2004).
147. M. Fabrizio, private communication.
148. R. W. Lof, M. A. van Veenendaal, B. Koopmans, H. T. Jonkman, and G. A. Sawatzky, *Phys. Rev. Lett.* **68**, 3924 (1992).
149. M. R. Pederson and A. A. Quong, *Phys. Rev. B* **46**, 13584 (1992).
150. P. A. Brühwiler, A. J. Maxwell, A. Nilsson, N. Mårtensson, and O. Gunnarsson, *Phys. Rev. B* **48**, 18296 (1993).
151. O. Gunnarsson, *Rev. Mod. Phys.* **69**, 575 (1997).
152. M. J. Rozenberg, *Phys. Rev. B* **55**, R4855 (1997).
153. R. M. Noack and F. Gebhard, *Phys. Rev. Lett.* **82**, 1915 (1999).
154. J. E. Han, M. Jarrell, and D. L. Cox, *Phys. Rev. B* **58**, R4119 (1998).
155. A. Georges, G. Kotliar, W. Krauth, and M. J. Rozenberg, *Rev. Mod. Phys.* **68**, 13 (1996).
156. O. Gunnarsson, E. Koch, and R. M. Martin, *Phys. Rev. B* **54**, R11026 (1996).
157. E. Koch, O. Gunnarsson, and R. M. Martin, *Phys. Rev. B* **60**, 15714 (1999).
158. M. J. Rozenberg, G. Kotliar, and X. Y. Zhang, *Phys. Rev. B* **49**, 10181 (1994).
159. M. Caffarel and W. Krauth, *Phys. Rev. Lett.* **72**, 1545 (1994).
160. O. Zhou, R. M. Fleming, D. W. Murphy, M. J. Rosseinsky, A. P. Ramirez, R. B. van Dover, and R. C. Haddon, *Nature (London)* **362**, 433 (1993).
161. R. Blinc, K. Pokhodnia, P. Cevc, D. Arčon, A. Omerzu, D. Mihailović, P. Venturini, L. Golič, Z. Trontelj, J. Lužnik, Z. Jegličič, and J. Pirnat, *Phys. Rev. Lett.* **76**, 523 (1996).
162. D. Arčon, P. Cevc, A. Omerzu, and R. Blinc, *Phys. Rev. Lett.* **80**, 1529 (1998).
163. V. Brouet, H. Alloul, T. N. Le, S. Garaj, and L. Forro, *Phys. Rev. Lett.* **86**, 4680 (2001).
164. J. Robert, P. Petit, T. Yildirim, and J. E. Fischer, *Phys. Rev. B* **57**, 1226 (1998).
165. A. Goldoni, L. Sangaletti, F. Parmigiani, G. Comelli, and G. Paolucci, *Phys. Rev. Lett.* **87**, 076401 (2001).
166. J. Schiessling, L. Kjeldgaard, T. Käämbre, I. Marenne, J. N. O'Shea, J. Schnadt, C. J. Glover, M. Nagasono, D. Nordlund, M. G. Garnier, L. Qian, J.-E. Rubensson, P. Rudolf, N. Mårtensson, J. Nordgren, and P. A. Brühwiler, *Phys. Rev. B* **71**, 165420 (2005).
167. K. Prassides, S. Margadonna, D. Arčon, A. Lappas, H. Shimoda, and Y. Iwasa, *J. Am. Chem. Soc.* **121**, 11227 (1999).

168. H. Tou, N. Muroga, Y. Maniwa, H. Shimoda, Y. Iwasa, and T. Mitani, *Physica B* **281**, 1018 (2000).
169. O. Zhou, T. T. M. Palstra, Y. Iwasa, R. M. Fleming, A. F. Hebard, P. E. Sulewski, D. W. Murphy, and B. R. Zegarski, *Phys. Rev. B* **52**, 483 (1995).
170. S. Margadonna, K. Prassides, H. Shimoda, Y. Iwasa, and M. Mézouar, *Europhys. Lett.* **56**, 61 (2001).
171. I. I. Mazin, S. N. Rashkeev, V. P. Antropov, O. Jepsen, A. I. Liechtenstein, and O. K. Andersen *Phys. Rev. B* **45**, 5114 (1992).
172. M. Lannoo, G. A. Baraff, and M. Schlüter, *Phys. Rev. B* **44**, 12106 (1991).
173. D. M. Deaven and D. S. Rokhsar, *Phys. Rev. B* **48**, 4114 (1993).
174. H. Y. Choi and M. J. Rice, *Phys. Rev. B* **49**, 7048 (1994).
175. O. Gunnarsson and G. Zwicknagl, *Phys. Rev. Lett.* **69**, 957 (1992).
176. L. Pietronero, *Europhys. Lett.* **17**, 365 (1992).
177. L. Pietronero, S. Strassler, and C. Grimaldi, *Physica B* **204**, 222 (1995).
178. E. Cappelluti, C. Grimaldi, L. Pietronero, and S. Strässler, *Phys. Rev. Lett.* **85**, 4771 (2000).
179. E. Cappelluti, C. Grimaldi, and L. Pietronero, *Phys. Rev. B* **64**, 125104 (2001).
180. M. Botti, E. Cappelluti, C. Grimaldi, and L. Pietronero, *Phys. Rev. B* **66**, 054532 (2002).
181. P. Paci, E. Cappelluti, C. Grimaldi, L. Pietronero, and S. Strässler, *Phys. Rev. B* **69**, 024507 (2004).
182. A. I. Lichtenstein, M. I. Katsnelson, and G. Kotliar, *Phys. Rev. Lett.* **87**, 067205 (2001).
183. O. Parcollet, G. Biroli, and G. Kotliar, *Phys. Rev. Lett.* **92**, 226402 (2004).
184. M. Capone, M. Civelli, S. S. Kancharla, C. Castellani, and G. Kotliar, *Phys. Rev. B* **69**, 195105 (2004).
185. J. E. Han, O. Gunnarsson, and V. Eyert, *Phys. Rev. B* **60**, 6495 (1999).
186. M. Capone, M. Fabrizio, and E. Tosatti, *Phys. Rev. Lett.* **86**, 5361 (2001).
187. I. M. Lifshitz, *Sov. Phys. JETP* **11**, 1130 (1960).
188. M. I. Katsnelson and A. V. Trefilov, *Phys. Rev. B* **61**, 1643 (2000).
189. R. Bulla, *Phys. Rev. Lett.* **83**, 136 (1999).
190. M. Capone, M. Fabrizio, P. Giannozzi, and E. Tosatti, *Phys. Rev. B* **62**, 7619 (2000).
191. M. Capone, M. Fabrizio, C. Castellani, and E. Tosatti, *Science* **296**, 2364 (2002).
192. B. Sutherland, *Phys. Rev. B* **12**, 3795 (1975).
193. Y. Q. Li, M. Ma, D. N. Shi, and F. C. Zhang, *Phys. Rev. Lett.* **81**, 3527 (1998).
194. S. Margadonna, K. Prassides, H. Shimoda, T. Takenobu, and Y. Iwasa, *Phys. Rev. B* **64**, 132414 (2001).
195. H. Kitano, R. Matsuo, K. Miwa, A. Maeda, T. Takenobu, Y. Iwasa, and T. Mitani, *Phys. Rev. Lett.* **88**, 096401 (2002).
196. E. Koch, *Phys. Rev. B* **66**, 081401 (2002).
197. M. Riccò, R. de Renzi, and A. Sartori, *Appl. Magn. Resonance* **19**, 517 (2000).
198. H. Shimoda, Y. Iwasa, and Y. Miyamoto Y. Maniwa, and T. Mitani, *Phys. Rev. B* **54**, R15653 (1996).
199. M. Riccò, T. Shiroka, A. Sartori, F. Bolzoni, and M. Tomaselli, *Europhys. Lett.* **53**, 762 (2001).
200. M. Riccò, T. Shiroka, E. Zannoni, F. Barbieri, C. Bucci, and F. Bolzoni, *Phys. Rev. B* **67**, 024519 (2003).

201. T. T. M. Palstra, O. Zhou, Y. Iwasa, P. E. Sulewski, R. M. Fleming, and B. R. Zegarski, *Solid State Commun.* **93**, 327 (1995).
202. H. Mori, M. Kamiya, M. Haemori, H. Suzuki, S. Tanaka, Y. Nishio, K. Kajita, and H. Moriyama, *J. Am. Chem. Soc.* **124**, 1251 (2002).
203. M. F. Craciun, S. Rogge, M. J. L. den Boer, S. Margadonna, K. Prassides, Y. Iwasa, and A. F. Morpurgo, *Adv. Mater.* **18**, 320 (2006).
204. R. W. I. de Boer, A. F. Stassen, M. F. Craciun, C. L. Mulder, A. Molinari, S. Rogge, and A. F. Morpurgo, *Appl. Phys. Lett.* **86**, 262109 (2005).
205. E. Tosatti, M. Fabrizio, J. Tobik, and G. E. Santoro, *Phys. Rev. Lett.* **93**, 117002 (2004).
206. We are grateful to M. Riccò for mentioning to us this possibility.
207. J. E. Han, O. Gunnarsson, and V. H. Crespi, *Phys. Rev. Lett.* **90**, 167006 (2004).
208. J. E. Han, E. Koch, and O. Gunnarsson, *Phys. Rev. Lett.* **84**, 1276 (2000).
209. M. Granath and S. Östlund, *Phys. Rev. B* **68**, 205107 (2003).
210. J. L. Dunn, *Phys. Rev. B* **69**, 064303 (2004).
211. M. Fabrizio and E. Tosatti, *Phys. Rev. B* **55**, 13465 (1997).
212. R. Martonák and E. Tosatti, *Phys. Rev. B* **49**, 12596 (1994); *ibid.* **54**, 15714 (1996).
213. C. A. Kuntscher, G. M. Bendele, and P. W. Stephens, *Phys. Rev. B* **55**, R3366 (1997).
214. P. Nozières and S. Schmitt-Rink, *J. Low Temp. Phys.* **59**, 195 (1985).
215. C. A. R. Sa de Melo, M. Randeria, and J. R. Engelbrecht, *Phys. Rev. Lett.* **71**, 3202 (1993).
216. J. E. Han, *Phys. Rev. B* **70**, 054513 (2004).
217. V. Buntar, H. Weber, *Supercond. Sci. Technol.* **9**, 599 (1996).
218. F. Vernay, K. Penc, P. Fazekas, and F. Mila, *Phys. Rev. B* **70**, 014428 (2004).